ADVANCED ELECTRONIC MATERIALS Open Access
www.advelectronicmat.de

State-of-the-Art Electronic Materials for Thin Films in Bioelectronics

*Imrich Gablech and Eric Daniel Głowacki**

This review is dedicated to electronics materials enabling thin-film-based neural interface and bioelectronics devices. First-generation bioelectronic medicine devices feature hand-crafted bulk interface electrodes, wires and interconnects, and insulators. This review discusses how modern materials science, especially know-how repurposed from semiconductor and microdevice technologies, enables next-generation bioelectronics. Those are divided into two subgroups: second and third generation. The former refers to rigid microscaled devices, while the latter is defined as soft, ultrathin, and flexible microdevices. A critical assessment of different biointerface electrodes, conductors for interconnects, and insulators for substrates, passivation, and encapsulation layers is made. The goal is not to give an exhaustive account of every use-example of given materials, but to point out specific aspects that are relevant to making the right choices for materials for a given device or application. Unique advantages of specific materials are highlighted, while also focusing on weaker points and caveats that those materials may have. The goal is to have an up-to-date handbook for persons entering the field which also points out tips and tricks as well as challenging problems that researchers can be inspired to confront and overcome.

1. Introduction

Bioelectronics and bioelectronic medicine represent growing fields where electrical interventions are used in the diagnosis and treatment of disease, often as a replacement or a supplement of pharmacology. The primary target of such therapies are neurological illnesses such as epilepsy, Parkinson's disease, chronic pain, and various movement disorders.[1] Other applications involve neuroprosthetic devices, which seek to restore lost function of the nervous system. Examples of such technologies include cochlear implants, retinal stimulators, and peripheral nerve interfaces for artificial limbs. The list of devices in clinical trials continues to grow, and new applications are emerging. This increasing demand puts new challenges in front of materials scientists and engineers. The field of bioelectronic medicine and neural interfaces relies on electronic materials which must conform to the strictest standards of robustness, safety, and reproducible electrical and electrochemical performance. The first generation of bioelectronic medical technology, developed already from the post-WWII period, relied on precision hand-crafted noble metal alloys (based on Pt, PtIr, etc.) and bulk insulator coatings of ceramics and silicone plastics or resins. While the materials science continues to evolve, the majority of devices used in the clinic today are primarily of this "First Generation," 1G, type. Examples are peripheral nerve electrodes, spinal cord stimulators, cochlear implants, or deep brain probes. In all cases, the bioelectronic interface consists of a bulk metal encapsulated with thick plastics, often with ceramic spacer layers. Many of these devices are assembled and tested by-hand by master craftsmen, working not unlike watchmakers. Since the 1970s, there has been an increasingly accelerating trend towards a "Second Generation" of bioelectronics (2G). What characterizes the 2G approach is using thin-film materials and processing techniques borrowed from the semiconductor industry to manufacture much smaller, more precise, and potentially more reliable and less invasive technologies. This idea has tremendous advantages. The first is scaling: wafer processing allows reproducible replication of numerous identical devices. The second is relative sizes of the resultant devices. Thin-film interface electrodes, conductive paths, and encapsulation/passivation layers can be processed down to sub-micrometer scale while retaining suitable electrical properties. This means that unlike 1G devices, with mm-scale thicknesses, 2G interfaces can be applied with total device thicknesses on the order of 1–100 µm.[2] This significantly lower thickness means smaller mechanical footprint and lower invasivity, as well as potential to target specific anatomical structures more finely. Moreover, there are indications that shrinking device sizes has positive implications for safety and biocompatibility, resulting in less scar tissue formation. The 2G approach has relied almost exclusively on silicon wafers as the substrate material. Monocrystalline silicon can be precisely microprocessed with nanometric precision. 2G silicon neural

I. Gablech, E. D. Głowacki
Bioelectronics Materials and Devices Laboratory
Central European Institute of Technology
Brno University of Technology
Brno 612 00, Czech Republic
E-mail: eric.daniel.glowacki@ceitec.vutbr.cz

The ORCID identification number(s) for the author(s) of this article can be found under https://doi.org/10.1002/aelm.202300258

DOI: 10.1002/aelm.202300258

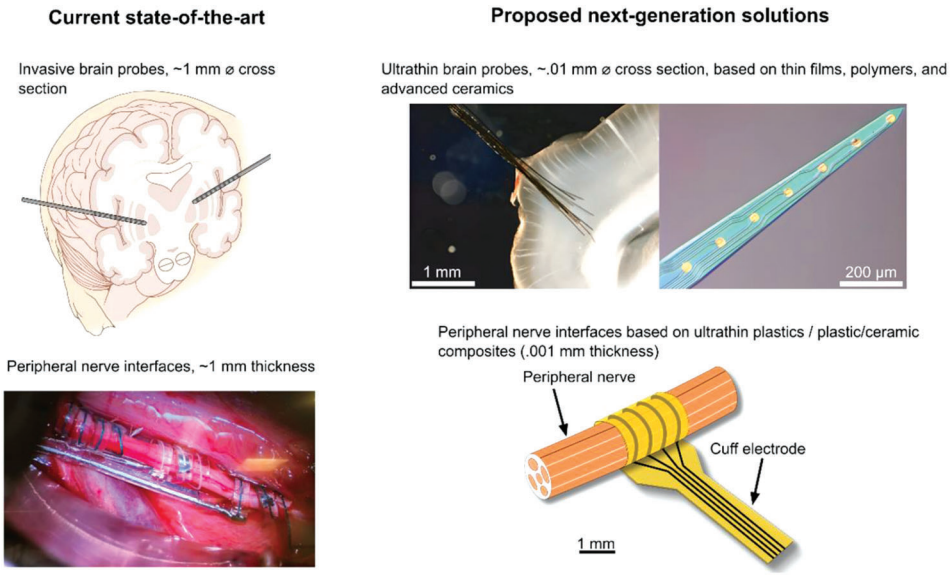

Figure 1. First generation (1G) devices in current medical practice are shown in the left column. Probes with multiple electrode contacts are made on the scale of mm thicknesses and lateral dimensions. Next generation (2G = rigid, 3G = soft/flexible) technologies are displayed in the right column.

interfaces are at the cutting edge of clinical translation, for instance, in the form of penetrating multielectrode arrays for brain–computer interfaces. At the level of fundamental neuroscience research, ultrathin silicon multisite probes have become the established standard for in vivo acute and chronic brain recording from experimental animals, and a range of systems is commercially available. The Si-based neural interfaces technologies are plagued by several drawbacks however. Silicon itself is brittle and rigid, and the mechanical mismatch with soft tissues leads to interfaces with poor chronic performance, as foreign body response is elicited by such probes. Silicon is also not stable in physiological conditions, and will corrode, necessitating careful passivation to prevent this effect. These mechanical and chemical considerations have led to a 3G set of approaches which rely on ultrathin flexible materials based on robust polymers or ceramics. These hold the promise of even less invasivity and are a logical choice for peripheral nerve "cuff" type devices.[3] While appealing, flexible 3G technologies suffer from much lower reproducibility than silicon technologies, and remain less technologically mature than Si processes. In short, many materials issues must still be resolved to make 3G devices reliable and competitive.

This review will cover electronic materials for thin-film-based neural interface and bioelectronics devices, namely, those referred to as 2G and 3G. While references will be made to state-of-the-art 1G devices, we will concentrate on what is enabling next generation technologies and what makes them different (**Figure 1**).

2. Bioelectronic Materials

2.1. Materials for Interface Electrodes

These materials must be electrically conductive and function as the charge transfer interface between the ionic environment of the physiological surroundings and the "dry" electronic circuit of the bioelectronic device. Interface electrodes are the critical component for both neurostimulation and recording. Key properties include: 1) good electrical conductivity. Especially for microdevices, series resistance of leads and electrodes must be minimized. 2) Low electrochemical impedance. Electrochemical impedance reflects the efficiency of charge transfer across the electronic/ionic interface, and is therefore fundamental for recording and stimulation. Recorded signals as well as stimulation impulses have frequency content typically in the range of 10–2000 Hz, thus this range will be important. 3) Excellent stability with respect to corrosion and ideally also biofouling. The next points, 4 and 5, are specific to stimulation electrodes only: 4) As large as possible electrochemically inert water window. This is the range of applied potentials in which irreversible electrochemical reactions do not occur; therefore, this is the range of potentials that can be safely applied to the electrode. 5) Charge storage capacity (CSC), and charge injection capacity (CIC). There is variance in the definition of these two concepts. Generally, this refers to the cathodic charge that can be transferred from the electrode to solution in a safe and reversible way, i.e., within the potential of the water window.[4] An effective stimulation electrode is one which can deliver a large amount of charge (or charge density) safely and reversibly without damage to the electrode or the surrounding tissue. The CSC is most commonly defined from the cyclic voltammogram of the electrode,[4a] where the integral charge under the cathodic part of the scan is regarded as "stored charge." Charge injection capacity, on the other hand, refers to the charge that is cathodically transferred during a short neurostimulation impulse, typically <1 ms in length.[5] Charge delivered up to the point where unsafe water-electrolysis voltages are reached is regarded as a practical limit of CIC. There are very large discrepancies between measurements of CSC and CIC in the literature, as different researchers define parameters differently. Moreover, measurement techniques and setups also are far

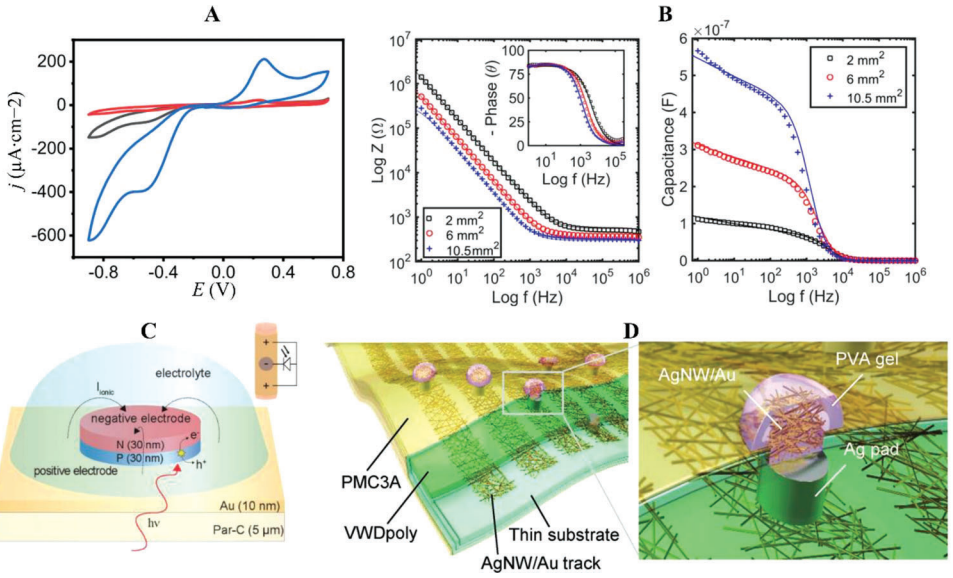

Figure 2. Gold. A) Cyclic voltammograms (100 mV s^{-1}) of a gold electrode in phosphate-buffered saline, with three conditions of oxygenation: nitrogen-purged (deoxygenated, red trace), ambient air (21% O_2, black trace), and oxygen-purged (100% O_2, blue trace). These scans demonstrate the affinity of gold for the oxygen reduction reaction. Drawn using data published in ref. [30c]. B) Impedance scans of evaporated gold thin films electrodes of various sizes, deposited on glass. This shows a gold/electrolyte interface as a high-pass filter, with moderate capacitance and moderate faradaic component at low frequency. Reproduced according to the terms of the CC CY license.[40] Copyright 2016, the authors, published by Springer Nature. C) Organic electrolytic photocapacitors (OEPCs) wirelessly stimulate the sciatic nerve in vivo and require a semitransparent bottom contact that has good adherence, good conductivity/transparency trade-off, and suitable stability. 10-nm thick gold films fulfill this role, using a Pd sticking layer to ensure good adhesion to the underlying parylene-c substrate. The Au exposed to physiological electrolyte should be encapsulated with a material to prevent anodic corrosion in chloride-containing environment. ITO or Ti is suitable. Figure adapted with permission.[34] Copyright 2022, Springer Nature. D) Au-coated Ag nanowires can be used to make competitive flexible MEAs for ECoG semitransparent arrays, providing light access for optogenetics as well as chronic stability for up to five months in vivo. Reproduced with permission.[35] Coypright 2019, Wiley VCH.

from unified. **Table 1** represents a survey of the electrode materials discussed in the following section, which can serve as a general guide to the state-of-the-art. Finally, general safety and biocompatibility apply to interface electrode materials as well as all materials constituting the implantable device. The ISO 10993 norm governs "Biological evaluation of medical devices" and describes how to test and score compatibility properties of medical devices, including implants. This should always be used as an established reference point when evaluating the compatibility of the electronic materials discussed in this review.

2.1.1. Metals and Their Compounds

Gold: Gold is well-known standard material thin film conductor used in electronic devices. Gold can be deposited remarkably easily by physical vapor deposition (PVD) techniques, namely, thermal evaporation or sputtering, and also can be chemically coated via electrochemical or electroless deposition techniques. Gold has one of the highest conductivities of any metal $\approx 4 \times 10^7$ S m^{-1} and relative to other high-conductivity metals like copper, silver, and aluminum it is chemically much more inert. Under ambient conditions, gold does not form an oxide layer and thus is regarded as a noble metal. This notion of gold stability and "nobility" holds true when considering normal "dry" electronics applications; however, this notion is not accurate in wet physiological conditions. In physiological solutions gold is remarkably electro(chemically) active. Under anodic polarizations in chloride-containing electrolytes, gold is susceptible to oxidative corrosion via the formation of soluble $AuCl_3^-$. Under cathodic polarizations, gold is highly electrocatalytically active with respect to the oxygen reduction reaction and cathodic water splitting. Due to electrocatalytic activity and chloride-assisted corrosion, gold itself is not suitable for neurostimulation electrodes due to its very narrow passive potential window. The presence of chloride ions and electrical potential causes electrodissolution of gold and the long-term device function with uncovered gold in chronic implants is essentially impossible.[28] Gold possesses high electrocatalytic activity for oxygen reduction reaction (ORR) with high selectivity for two-electron oxygen reduction to hydrogen peroxide (**Figure 2**a). The hydrogen peroxide evolution on gold thin films was found to be as maximal for (111) oriented Au surfaces.[29] The generation of peroxide on exposed gold thin films may be a confounding factor in certain bioelectronics devices. It is not possible to perform stimulation without unwanted accompanying chemical reactions which are potentially harmful for tissues due to the production of toxic hydrogen peroxide under very low cathodic polarizations of a few hundred millivolts.[30] It should be said that this phenomenon of peroxide and reactive species generation has been proposed, on the other hand, to be an interesting strategy for biological experiments.[31] Gold thin films have relatively low specific capacitance around 10–20 μF cm^{-2}, with impedance being dominated by faradaic reactions at low frequency (Figure 2b).

In microfabricated bioelectronics, without question gold is the most popular conductive material for encapsulated conductive

Table 1. Survey of charge storage capacity (CSC) and charge injection capacity (CIC) reported for different neurostimulation electrode materials. While impedance values will differ with electrode size and cannot be reliably normalized, CSC and CIC are normalized to electrode geometric area in cm^2. Despite this, quantitative comparison of these values should be considered with caveats, as measurement techniques and assumptions on "safe" water window values differ across the literature.

Material	Preparation method / sample structure	CSC [mC cm^{-2}]	CIC [mC cm^{-2}]	Charge injection mechanism	Ref.
Au	Microdots	2	1.9 (0.4 V bias)	Capacitive double layer + Faradaic	[6]
	Thin film	–	1.27		[7]
	Thin film	0.103 ± 0.015 (CSC_C)	0.02		[8]
IrO_x	Sputtering (SIROF)—thin film on UTAH electrodes	100	5	Pseudofaradaic- – reversible changes of the valance state of Ir	[9]
	Electrodeposited (EIROF) on C fiber	48.7 ± 1.2 (CSC_C)	1 (0 V bias) 17 (1 V bias)		[10]
	EIROF on Pt thin film	12 (CSCc)	2		[11]
	Comparative study of site electrodes SIROF EIROF AIROF (activated IROF)	36.15 68.20 40.07	–		[12]
Pt and PtIr alloys	Sputtered Pt Sputtered PtIr (55:45) (both thin films)	16 22	–	Capacitive double layer + Faradaic	[13]
	PtIr tube alloy (90:10)	16.8 (rough) 1.1 (smooth)	–		[14]
	Pt disc	–	0.003–0.054		[15]
	Pt thin film	3.18 (CSC_C)	0.08 ± 0.02		[11]
	Pt thin film (roughened)	–	1.39		[16]
TiN	Thin film	2.35 (CSC_A) 2.47 (CSC_C)	0.9	Capacitive double layer	[17]
	Porous thin film	22–53 (in PBS based on scan rate)	–		[18]
	Thin film	-	4.45 (electrode voltage of −3 V and bias of −0.8 V)		[19]
C and its allotropes	Printed graphene	31.3	0.43	Capacitive double layer + pseudofaradaic	[20]
	CNT-based MEAs	1.2	0.5		[21]
	Glassy carbon microelectrodes	61.4 ± 6.9	3		[22]
PEDOT	Electropolymerized on site electrodes (PEDOT:PSS)	75.6 ± 5.4	5	Pseudofaradaic- – reversible changes of the redox state of the PEDOT backbone, with counter ions transported in and out of the film	[23]
	Spin-coated (PEDOT:PSS)	17.71	2		[24]
	PEDOT:PSS hydrogel (13 vol% DMSO)	60	8.3		[25]
	Electropolymerized (on Pt thin film) PEDOT:PF_6 PEDOT:ClO_4 PEDOT:PSS	80.1 ± 6 36.6 ± 1.8 18.4 ± 1.23	–		[26]
PPy	Electrodeposition (on Pt wire) PPy/Cl PPy/PSS PPy/SWCNTs	CSC_A / CSC_C 317 / 495 444 / 705 785 / 1244	3.2 5.0 7.5	Pseudofaradaic – reversible changes of the redox state of the PPy backbone, with counter ions transported in and out of the film	[27]

leads, because the electrical conductivity is still unbeaten.[32] Furthermore, gold has also excellent conductivity even at very low thickness under ≈10 nm. Such films are conductive and also semitransparent, giving optical transmission in the range from 40% to 60% in the visible spectrum.[33] This feature is exploited in the fabrication of photocapacitors for wireless peripheral nerve stimulation (Figure 2c) Ultrathin gold is used as a return electrode, versus a primary stimulation electrode comprising organic semiconductors on a flexible parylene substrate.[34] Gold on flexible substrates appears to be a good solution, but it brings the issues of poor adhesion on polymeric substrates, thus, it must be combined with appropriate adhesion layers such as Cr, NiCr, Pd, ITO, or Ti. These thin interlayers help to ensure good adhesion on the polymeric substrate without sacrificing transparency. This example of photocapacitors also highlights gold electrochemical stability in physiological media. The areas of gold which are in direct contact with the surrounding media are, for chronic applications, encapsulated with a thin layer of indium tin oxide (ITO). Another approach to achieving semitransparency while maintaining high conductivity is to prepare high-aspect-ratio nanowires. Araki et al. demonstrated impressive long-term in vivo stability (up to five months) in cortical recording from nonhuman primates using Au-coated Ag nanowires. These are solution-processable suspensions, which the authors patterned onto flexible plastic substrates, achieving good recording performance and optical transparency. They prevented the problem of fouling of the gold surface by using hydrogel coatings.[35] It is important to mention that the chemical properties of gold allow easy functionalization, via the formation of sulfide bonds between free thiol (–SH) groups and the gold surface. This can be used to covalently attach adhesion layers for crosslinkers and enzymes in biosensors, for instance, in the application of mRNA detection.[36] Moreover, thiol chemistry can be used to make excellent sticking layers onto which gold can be deposited, presenting a good alternative to underlayers like Cr.[37] Due to its electrocatalytic properties, gold can be used for nonenzymatic electrochemical sensing of glucose.[38] Another application of gold is as a substrate for conducting polymer electrodes. Gold is a suitable electrode for electrochemical polymerization of conducting polymer monomers, such as 3,4-ethylenedioxythiophene (EDOT). Gold ensures sufficient electrical contact and conducting polymers have good adhesion on gold surfaces.[39]

Hafnium Oxide: HfO_2 is well known for its high-*k* dielectric constant and is used in fabrication of CMOS integrated circuits and memory devices. It can be prepared by both chemical vapor deposition, (CVD) and PVD methods. Though it is an insulator, it is usable as an interface electrode material due to its high dielectric constant and thus high capacitance. Furthermore, in its ferroelectric crystallographic phase, it could afford even higher charge injection capacity. The notion of using dielectric oxides (TiO_2, ZrO_2, Ta_2O_5, etc.) as purely capacitive interfaces for ultimate "safe" non-faradaic extracellular stimulation has been championed by various researchers, with Fromherz being the most notable proponent.[41] He utilized multielectrode chips with Si/HfO_2 capacitor pixels for capacitive extracellular stimulation. Charge injection can be further boosted exploiting ferroelectric phases in HfO_2. It should be noted that to reach optimal crystallography during deposition or during postprocessing usually requires elevated temperatures which can be problematic for flexible substrates.[42] Exploiting ferroelectric materials for stimulation microelectrodes was evaluated in a theoretical study by Becker. This study considered the ferroelectric $Hf_{0.5}Zr_{0.5}O_2$ oxide. It was calculated to possess charge injection capacity on the order of tens of μC cm^{-2} for thickness of 9.5 nm while the electrode diameter was 50 μm. A further material of interest behaving similarly was $Al_{1-x}Sc_xN$.[43] It is necessary to mention that real results can be different from these models. In general, the idea of high-*k* interface electrodes for stimulation remains largely untested, and one practical issue is the difficulty in fabricating pinhole-free layers with high dielectric strength at such low thickness on electrode areas in hundreds or thousands of μm^2. This requires extremely clean and well-optimized conditions which are difficult to accomplish in academic research laboratories. These same issues also plague passivation/encapsulation layers, as will be discussed later in this review.

Iridium Oxide: Iridium oxide, normally denoted as IrO_x, refers to a mixture of metallic iridium and different valences of iridium oxide. It can be prepared via electrodeposition, anodization of metallic iridium layers (often referred to as "activation" in the literature), and via PVD (reactive sputtering), or CVD, in a wide range of different temperatures.[44] Among bioelectronics electrode interface materials, IrO_x is renowned for low impedance and high charge injection capacity.[45] The high charge capacity is connected to the pseudofaradaic phenomenon of IrO_x as a valence-change oxide.[46] This means application of electrochemical potential drives reversible redox reactions within the IrO_x layer itself, leading to extraordinarily values of charge capacity. This capacity can be further enhanced by tuning the preparation method and its parameters to increase layer roughness and porosity, thereby leading to increase in active surface area.[44b,47] The measured electrochemical capacitance of IrO_x thin films can reach units of mF cm^{-2} which represent some of the highest values reported for thin film materials (**Figure 3**). In microfabricated 2G and 3G type devices, sputtered IrO_x (commonly referred to as SIROF) is the most popular, by virtue of reliable fabrication and also, according to many reports, superior performance versus IrO_x prepared by other routes. This material has been involved in many applications such as depth probes, "Utah style" multisite probes for stimulation and recording, and cuff electrodes or MEAs.[48] In a macroelectrode application, Lee et al. compared IrO_x, with Pt and Ir on cuff electrodes for rat sciatic nerve stimulation using an electrode diameter of 0.8 mm. All materials were prepared using magnetron sputtering on polyimide substrates. The impedance at 1 kHz of IrO_x was 0.72 kΩ which is higher than for Pt 0.48 kΩ, but the charge injection capacitance reaches the value of 60 mC cm^{-2} which was several times higher than the value for Pt, or pure Ir. Unlike the faradaic behavior of Pt, in cyclic voltammograms of IrO_x, reversible pseudofaradaic behavior was apparent in the range from −0.7 to +0.7 V.[49] IrO_x microelectrodes for stimulation have proven to be effective in chronic applications, one remarkable example being as stimulation electrodes in photovoltaic retinal implants. These have been successfully tested in animal models and have shown success in a large clinical trial, where implants are functioning for more than a year.[50] From the point of view of harmful faradaic reactions, IrO_x does catalyze the oxygen reduction reaction;[51] however, among a series of materials studied in biphasic stimulation protocols, IrO_x produces the least hydrogen peroxide as a byproduct.[30c]

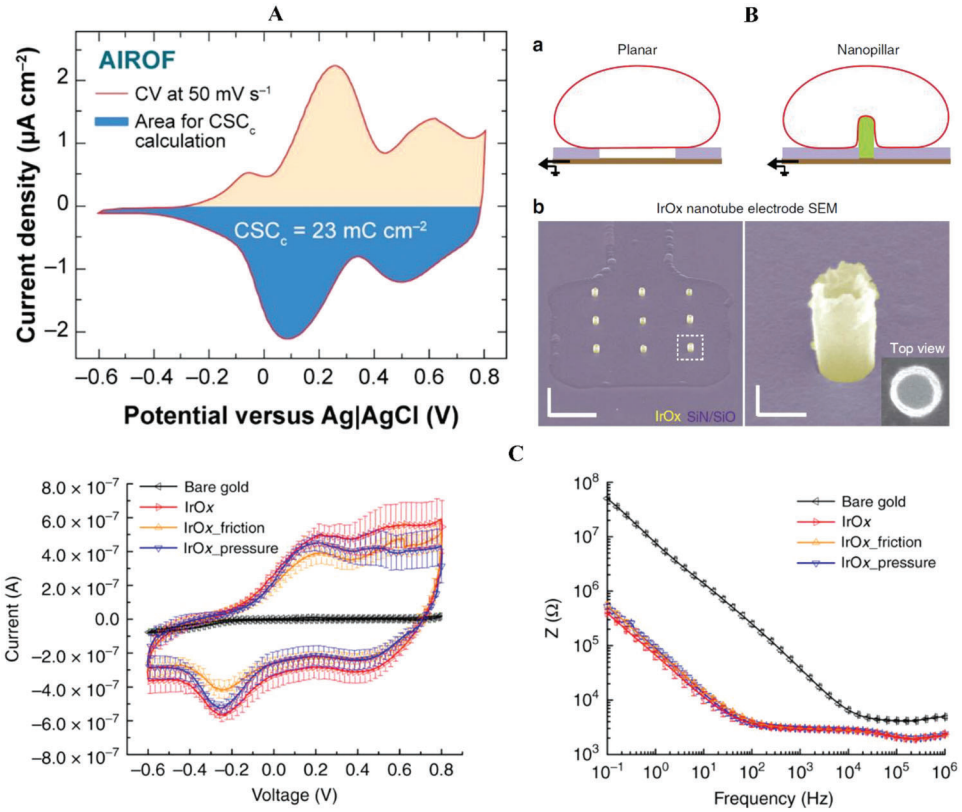

Figure 3. IrO_x. A) Cyclic voltammogram of an activated (anodized) iridium oxide sample, showing the characteristic pseudofaradaic peaks corresponding to redox reactions between the different valence states of Ir. The integrated cathodic current is defined as the charge injection capacity, *aka* charge storage capacity, CSC. Reproduced with permission.[4a] Copyright 2008, Annual Reviews. B) Iridium oxide nanopillars (200 nm diameter) deposited by electrodeposition from iridium chloride solution can perform high-quality single cell intercellular recording from MEA electrodes. Right scale bar = 200 nm. Reproduced according to the terms of the CC BY license.[52] Copyright 2014, the authors, published by Springer Nature. C) Cyclic voltammogram and impedance recording of sputtered IrO_x electrodes subjected to various treatments, compared with gold as a reference. The charge storage capacity is clearly much higher in the IrO_x case, which also corresponds to the lower impedance values. Reproduced according to the terms of the CC BY license.[53] Copyright 2018, the authors, published by Springer Nature.

Platinum and Platinum–Iridium Alloy: Platinum is known as a noble metal and is eminent as an electrocatalytic material. It has high electrical conductivity.[54] Platinum is usually prepared with PVD methods like evaporation, magnetron, or ion-beam sputtering at ambient temperature. Preparation using CVD methods is also possible. Platinum electrical resistivity is only ≈3× higher than the resistivity of gold, making it a suitable choice for many interconnect applications. Its remarkably stable electrical resistivity is demonstrated by its use as the resistor layer in ultrathin resistive temperature-sensing layers.[55]

Compared to other electrode interface materials in bioelectronics, Pt and Pt-Ir hold the leading position in 1G and 2G devices. Pt-Ir alloy in the form of bulk samples (i.e., wires, sheets, etc.) is the most well-established material for clinical implantable bioelectronics like deep brain stimulators and vagus nerve stimulation electrodes. The majority of implanted bioelectronic devices feature Pt or a Pt alloy. The addition of Ir to the alloy with Pt is not for electrochemical performance reasons, but rather to increase the mechanical resilience of Pt, which is otherwise too soft to work with in bulk form. Pt is used in numerous neural interfaces applications for stimulation primarily, such as deep brain stimulation, cochlear implants, and similar. There are less examples where Pt is employed for high-performance recording applications, however clinical electroencephalography (EEG) grids are normally made with Pt electrodes. As a neurostimulation material, charge injection with Pt is primarily faradaic. Due to the electrocatalytic properties of Pt, it is widely assumed that faradaic reactions occurring at the Pt can be relatively reversible. While Pt is relatively stable over long periods of time, electrode performance can be decreased because of protein adsorption,[55c] and Pt is also prone to form soluble chloride salts, leading to anodic dissolution at higher potentials. While the double layer capacitance of Pt is modest, there are techniques to drastically increase the geometric surface area of Pt and thus obtain highly porous, high-capacitance electrodes. The surface of Pt can be roughened by laser ablation or electrochemical treatment.[16,56] Record-high capacitance can be obtained by electrodeposition of Pt (so-called nano-Pt, **Figure 4**). This technique leads to complex, hierarchical nano/microstructures with extremely high surface area and also outstanding stability with respect to electrical and chemical stressing. Another method to yield porous Pt layers of comparable performance is by reduction of sputtered PtO_x films, a method that is easily compatible with a microfabrication

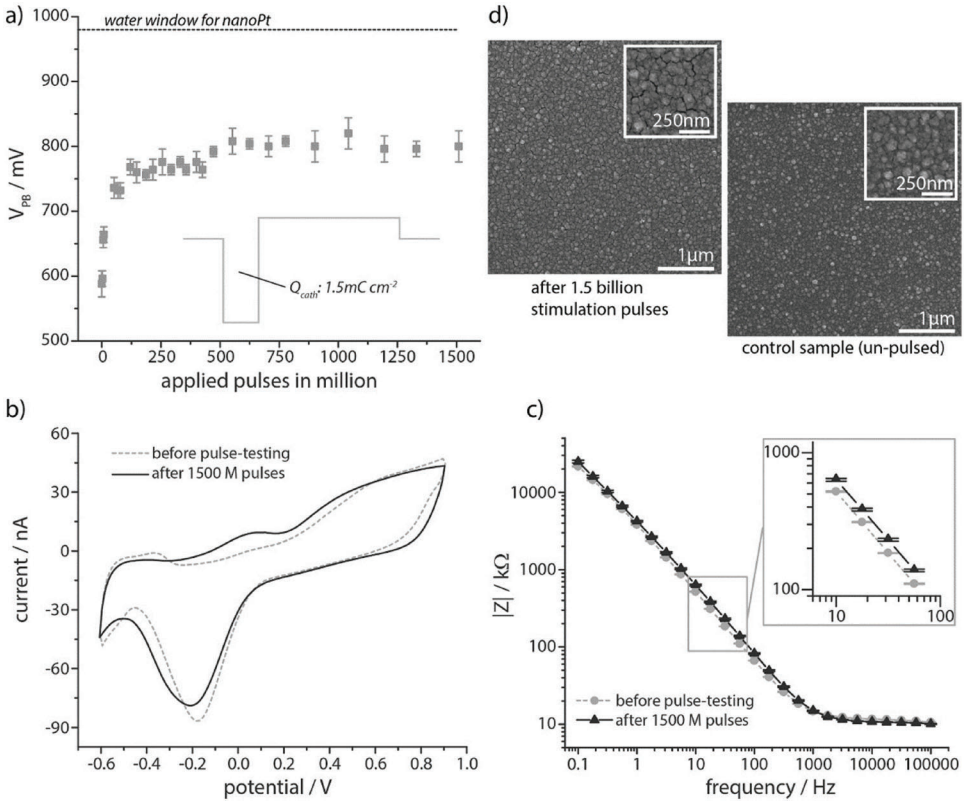

Figure 4. Platinum. These measurements are for long-term stability tests for nanostructured electrodeposited Pt layers known as "NanoPt," fabricated on 35 µm diameter microelectrodes, reproduced with permission.[59] Copyright 2020, ACS. a) Voltage excursion during application of a 1.5 mC cm^{-2} stimulation pulse, demonstrating stable and safe charge injection over a billion cycles. The morphology, cyclic voltammetry, and impedance shown in subsequent panels clearly do not change over a billion cycles of stressing. This showcases the promising stability of platinum, even in a nanostructured form.

process.[57] Due to its electrocatalytic properties and thus propensity for driving reversible faradaic reactions, Pt is more popular for fabrication of EEG electrodes utilized in stimulation devices. However, most of the applications such in vivo stimulation needles, oxygen sensors, or cancer treatment tools are not used for long-term experiments.[58]

While Pt-Ir is normally deployed in its bulk form, it can also be processed in thin films. According to some reports, Pt-Ir alloys exhibit performance superior to pure Pt, for both neurorecording and neurostimulation. The alloy has lower impedance values over a broad frequency range.[14,60] The most-used method for preparation is magnetron cosputtering from Pt and Ir targets which gives good control of Pt and Ir content in the alloy film. Deposition of this type does not require additional heating, which makes it suitable for flexible devices.[49] Pt-Ir can also be prepared by electrodeposition, which was published by Cassar et al. They improved commercial penetrating MEAs and proved significant performance increase in comparison to the commercial one with promising results during long-term in vivo tests in rat brain.[61] Furthermore, Pt-Ir prepared by electrodeposition was utilized on carbon microfiber electrodes (**Figure 5**) with tip diameter of ≈2 µm by Valle et al. They successfully deployed these devices in vivo in rat brains, and reported a charge injection capacity of 1.25 mC cm^{-2} using 0.5 ms pulses in PBS within the passive water window.[62]

Titanium: Titanium possesses excellent biocompatibility and is often used in biomedical implants as a robust structural material. For thin film 2G and 3G devices, titanium is frequently used as adhesive layer for other metals or polymers, but rarely as an interface electrode. While pure titanium has roughly 3× lower conductivity than gold, thin film titanium is nearly always prepared in vacuum systems with imperfect vacuum and deposited films have high oxygen content and significantly lower conductivity than the "textbook" values for Ti. Hence, it is not suitable for long leads as the main conductive material. Titanium is however a well-known adhesion layer for Au, Pt, and also for conducting polymer and diamond-like carbon coatings. Furthermore, Ti can be also used as top-covering layer for gold or platinum to promote adhesion of subsequently deposited Parylene-C. Since it forms a stable surface oxide, that oxide can be relied upon for chemical functionalization with linker molecules like silanes, which is a convenient feature in designing a reliable multimaterial stack. Use of titanium as a neural interface electrode has been explored only minimally. Titanium forms a highly stable semiconducting oxide on the surface, and it has been suggested that anodized Ti/TiO_2 can be used for purely capacitive stimulation electrodes. Titanium microwires used for in vivo brain recording and stimulation have been reported, with an anodized TiO_2 coating. These gave capacitive charge injection capacities of 60 µC cm^{-2}.[41a] Considering the extremely high

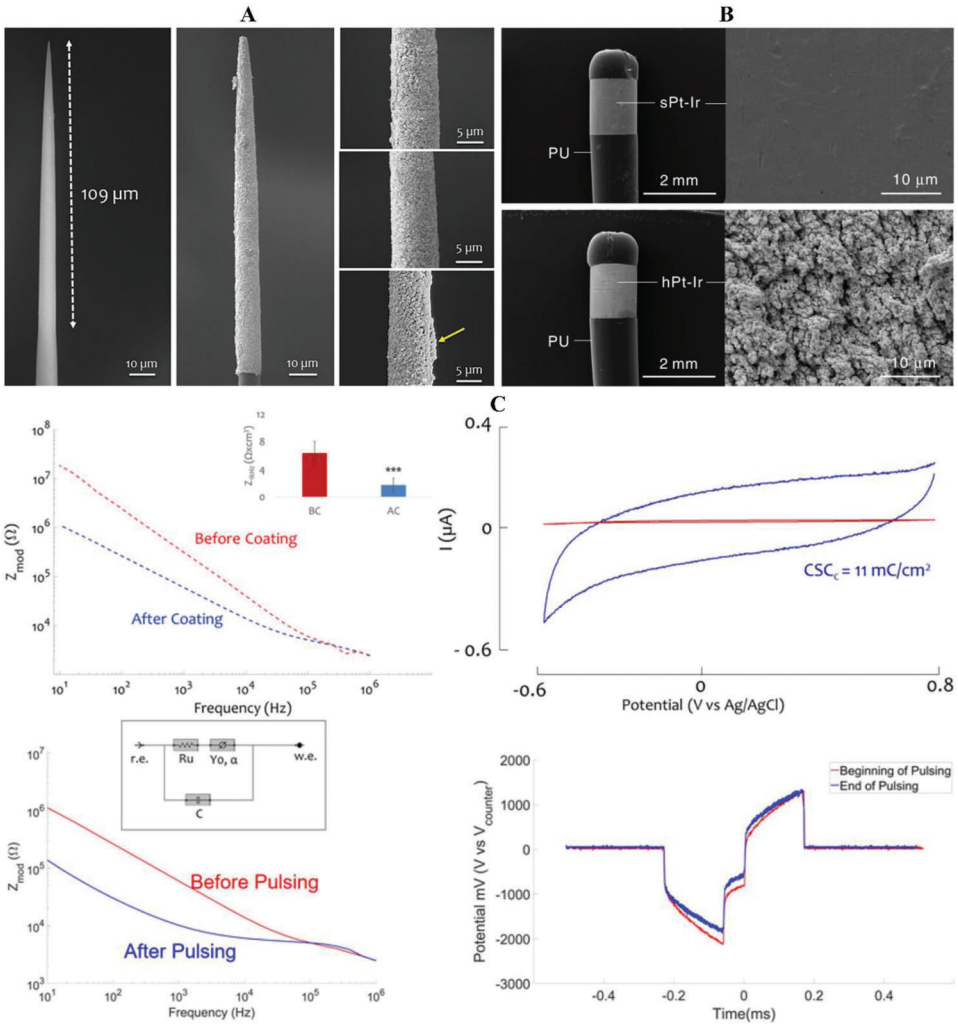

Figure 5. Pt-Ir. A) Scanning electron microscopy of a carbon fiber before (left) and after the PtIr coating (middle); and (right) SEM images of three different PtIr-CF coatings.[62] B) Smooth and hierarchical Pt-Ir electrode surfaces on a penetrating probe electrode (sPt-Ir and hPt-Ir). Reproduced according to the terms of the CC BY license.[14] Copyright 2022, the authors, published by Springer Nautre C) Electrochemical characterization: electrochemical impedance spectroscopy (EIS) measurement (top left) of one sharpened carbon fiber before and after the plating process; as inset the mean and standard deviation of the normalized impedance are reported before (red) and after (blue) the coating. (Top right) Cyclic voltammetry (CV) of a sharpened carbon fiber before (red) and after (blue) the PtIr plating process, the cathodic charge storage capacity of the electrode increases to 11 mC cm^{-2} after the coating (0.2 mC cm^{-2} before the coating). 300 Hz electric pulse test: EIS (bottom left) of one PtIr-CF before (red solid line) and after (blue solid line) pulsing on Day 1; as inset the circuit model used for fitting impedance data is shown. Voltage transient (bottom right) for one PtIr-CF in the beginning (red) and at the end of pulsing test (blue); a biphasic pulse of 170 µs duration and amplitude of 105 µA (1 mC cm^{-2}) was applied. Reproduced according to the terms of the CC BY license.[62] Copyright 2021, the authors, published by Frontiers.

number of studies on nanostructured anodized titania in the materials science field, it is surprising that this has not been more explored in the context of neural interface electrodes.

Titanium Nitride: Titanium nitride is an excellent ceramic material in terms of crucial properties for bioelectronics like electrical conductivity, (electro)chemical stability, and biocompatibility. In its stoichiometric form, TiN has higher conductivity than pure Ti metal. Coatings prepared by sputter deposition can form rough and highly porous structures with high surface and high capacitance, and were already used extensively in coating of bulk electrodes in 1G devices, such as cardiac pacemaker electrodes.[63] Porous magnetron-sputtered titanium was published in 1998 for MEAs for in vitro neuroscience research, and to-date TiN MEAs of this type remain a standard in the field (**Figure 6**a).[64] Since that time, TiN has been lauded as a stable material with capacitive charge injection, which can be enhanced via the preparation of porous structures. The overall charge injection capacity of porous TiN is not as high as pseudofaradaic materials like IrO_x and PEDOT, but it can be suitable for many applications. At present, well-prepared TiN can compete with materials like IrO_x or Pt because of its low-price and notable chemical resistance and biocompatibility. It possesses excellent compatibility with many types of cells, and thus can serve as good electrode layer for cell cultivation with long-term recording/stimulation.[65] TiN has been successful in chronic devices for neurorecording and neurostimulation.[66] The most highly-optimized system

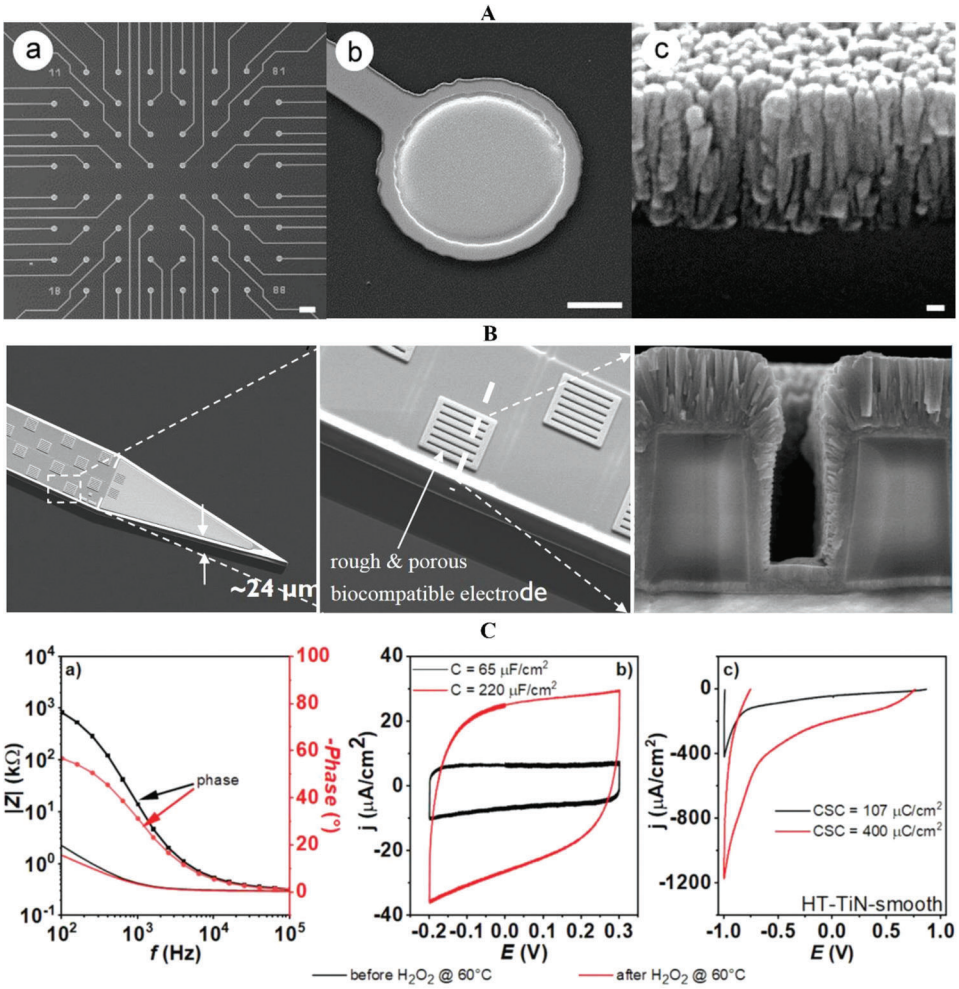

Figure 6. TiN. A) Magnetron sputtered TiN MEAs, with cross-sectional electron microscopy showing the rough columnar morphology of these TiN layers, which feature competitive impedance and high charge injection capacity. Reproduced with permission.[69] Copyright 1998, Elsevier. B) Multisite brain probe "NeuroPixels 2.0" TiN microelectrodes of 144 µm^2 size, with recording-setting impedance values. Low impedance is maintained via a rough surface morphology of the TiN as well as microengineered pores to further increase surface area. Reproduced with permission.[70] Copyright 2019, IEEE. C) Impedance and cyclic voltammetry data of stoichiometric TiN films prepared by high-energy ion beam sputtering, before and after treatment with hydrogen peroxide. Partial oxidation of the TiN surface clearly increases the capacitance by a factor of nearly 4×. Reproduced according to the terms of the CC BY license.[71]Copyright 2023, the authors, published by Wiley VCH.

to-date is the Neuropixel 2.0 recording and stimulation system. It features up to thousands of channels comprising TiN porous thin-film microelectrodes, each with an area of 144 µm^2. These microelectrodes achieve an impedance of 150 kΩ at 1 kHz, which is extremely competitive for such a small electrode (Figure 6b).[67]

The actual materials science details of these competitive TiN systems are not publicly known. What is clear is that there is a wide range of actual stoichiometry and crystallinity of "TiN" materials which appear in the literature and different applications. Most, if not all, to-date reported TiN formulations contain oxynitride TiON phases to a lesser or greater degree. Preparation of stoichiometric of TiN is challenging, especially at low temperatures. Oxygen contamination in sputtering systems is essentially inevitable, and Ti is well-known getter material in vacuum technology. Many papers exist about the optimization of TiN deposition process, but the reported parameters are usually very different between publications. TiN deposition is highly dependent on parameters such as: underlayer morphology (roughness and crystallography), vacuum purity, substrate temperature, and particle energy. In general, last two mentioned parameters have the most significant influence on adatom energy which is important for layer properties.[68] Not surprisingly, the impedance and capacitance values published in papers on TiN for bioelectronics can vary by one or two orders of magnitude. Also, the passive water window can vary by several hundred millivolts.[68c] Stoichiometric TiN prepared by high-energy ion-beam sputtering has roughly ten times higher conductivity than commercial porous "TiN", however has significantly lower charge injection capacity. However, after oxidative treatment of these films with hydrogen peroxide, charge injection capacity increases greatly, and impedance drops (Figure 6c). This indicates that some level of

oxidation and oxynitride is tied to desired low-impedance properties of TiN.

For 3G devices, preparation of TiN on flexible polymeric substrates like Parylene-C and polyimide is challenging. This is because deposition must be done within a limited thermal budget, and TiN has a relatively high Young's modulus and common residual stress which can reach values lower than −1 GPa.[66] This latter effect can cause unwanted deformation of plastic substrates. These limitations are problematic to obtain high-performance TiN on flexible substrates.

Tungsten: W is a famous material in bioelectronics due to the ease of preparation of finely sharp microneedles via electropolishing. Such microelectrodes are a classic brain probe for acute single-unit recording, and are commercially available for this purpose. For chronic recording/stimulation applications, W cannot be used due to its rapid corrosion in biofluids.[72] However, it has been argued that the solubilized forms of tungsten arising from corrosion are not toxic or harmful. This property, combined with high electrical conductivity and ease of microprocessing, has led tungsten to be the enabling material for the emerging field of bioresorbable electronics.[73] Bioresorbable electronics, also known as transient electronics, are meant to be implanted, function for a period of time, and then degrade in a programmed way.[74] For such devices, tungsten is an attractive conductor material. On top of this, tungsten has been explored in other forms like WS_2 nanosheets or nanotubes to improve properties of bioresorbable scaffolds.[75] The oxide WO_3 is a thin film n-type semiconducting material which has been suggested for use biosensors and nonenzymatic peroxide detection.[76]

Liquid Metal Eutectics: Metallic conductors are fundamentally stiff and brittle to a great degree, and care must be taken in the design of all bioelectronic devices to create metallic interconnects in a way to effectively accommodate the desired degree of flexibility. One may to circumvent this problem is to use metallic materials that are intrinsically flexible, stretchable, and conformable: liquid metals. While the elemental metal Hg is a room temperature liquid metal, it is far too toxic for consideration in any applications. A much more suitable candidate is gallium. The melting point of Ga is 29 °C, making it a liquid with a viscosity roughly twice that of pure water. This allows Ga to be used as liquid metal at physiological temperatures. For processing, however, dropping the melting point below room temperature is desirable. It is possible to prepare various eutectic mixtures of Ga with In, Sn, Pb, Cd, etc. For practical and safety reasons, eutectic GaIn, known as EGaIn, is by far the most popular liquid metal tested in the context of bioelectronic devices.[77] EGaIn, as a liquid metal, can fill a microfluidic channel and thereby create a metallic conductor that fills the shape of the channel. With this approach, by using elastomeric microfluidics one can obtain metallic interconnects that are highly flexible and stretchable, and even self-healing after mechanical cutting of such a liquid metal interconnect. Another considerable added value of EGaIn is that it can impart excellent hermeticity to elastomeric plastics, as with respect to gas transmission it has the barrier properties of a metal. In on-skin (non-implanted) devices, there have been many successful demonstrations of liquid metal electrodes which leverage the excellent mechanical properties of the liquid metal. As a neural interface electrode, EGaIn has been explored only minimally. In 2012, a seminal report on the topic demonstrated the possibility of using EGaIn electrodes in a MEA chip for in vitro neurostimulation.[78] In the work of Latif and colleagues EGaIn in a flexible conduit was tested as a neural stimulation electrode, and was reported to have charge injection capacity and impedance values about an order of magnitude superior to gold thin film reference samples.[79] However, the long-term electrochemical stability in physiological media of such electrodes remains to be established, as well as fundamental properties like charge injection capacity should be definitively studied. Another remaining issue is the in vivo toxicity of gallium, indium, and other metals used in such eutectics. This topic has been recently reviewed and in the context of neural applications remains an open question.[80]

2.1.2. Organic materials

Carbon and Its Allotropes: Carbon exists in many forms, with various levels of electrical conductivity and diverse electrochemical properties. As a general rule, carbon electrodes display (usually) low faradaicity due to sluggish charge transfer kinetics in processes like water splitting. Various graphite and glassy carbon electrodes, in bulk form, are commonly used in bioelectrochemistry. Carbon electrodes typically have excellent electrochemical stability and corrosion resistance. Thin film carbon-based devices have begun to be explored extensively in recent years. Carbon can be deposited by PVD or CVD methods in the form of glassy thin films, or various 2D and 3D nanostructures such as nanotubes, graphene, buckminsterfullerene, or diamond-like carbon thin films. These represent different allotropes of the element carbon.[81]

Sputtered carbon thin films doped with varying boron concentrations are well-known in the field of biosensors. Kaivosoja et al. employed carbon based thin films for dopamine levels detection in neural sensing. Preparation was done using unbalanced magnetron at room temperature, which can be crucial for many flexible devices. These electrodes have a wide water window in range broader than ±1 V while the capacitance was in the range from 50 to 100 μF cm^{-2}.[82] Due to the low background of faradaic reactions, such electrodes can be used for redox detection of sensitive analytes like dopamine.

Graphene, as a topic of study, is the most popular carbon allotrope due to its excellent electrical and mechanical properties studied in many fields such as FETs, gas sensors, strain sensors, etc. It is not surprising that graphene has been tested for in vitro and in vivo use as a neural interface electrode, for both stimulation and recording. While graphene can display impressively low impedance and moderate charge injection capacity when processed into high surface-area 3D structures, many studies have pointed out issues of biocompatibility and possible cytotoxicity.[83] An attractive emerging technique is that of laser-induced graphene conductors/electrodes. In this method, laser energy is used to pyrolyze insulating engineering polymers like polyimide, producing conducting traces of pyrolyzed graphene. This way, high surface-area electrodes can be patterned directly into a suitable substrate. Such rough graphene layers can be easily functionalized with conducting polymer coatings to further decrease impedance.[84]

Diamond-like carbon (DLC) is semiconductive form of amorphous carbon with sp^3 bonding. DLC possesses high mechanical

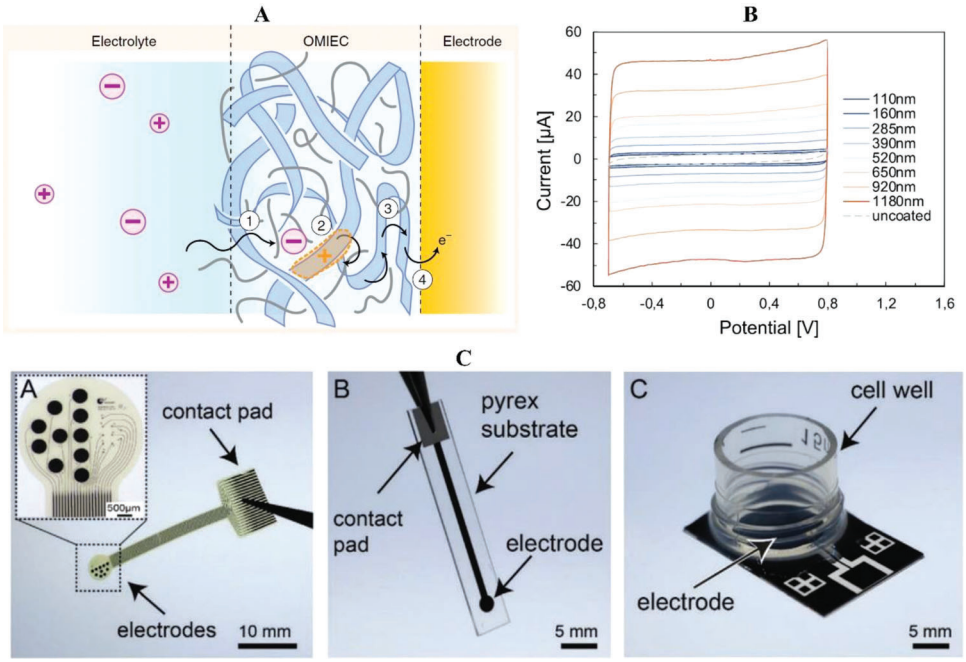

Figure 7. PEDOT. A) Schematic illustration of the charging mechanism of an interface of electrolyte/organic mixed ionic-electronic conductor (OMIEC)/electrode. This applies to PEDOT and related materials. Electronic charges move through the conjugated polymer backbone and can be transferred to an underlying metal electrode. Meanwhile, ions can migrate into the PEDOT layer to balance the electronic charge on the backbone. This charging effect, with accompanying ion transport, occurs throughout the whole bulk of the PEDOT, thus leading to the effect of volumetric capacitance. This figure is reproduced with permission.[88b] Copyright 2020, Springer Nature. B) Cyclic voltammetry of PEDOT films deposited on gold underlying contacts, showing how the capacitive charge of the electrode corresponds to the thickness of the PEDOT, a clear evidence for the effect of volumetric capacitance. Reproduced with permission.[97] Copyright 2020, Wiley VCH. C) Examples of test structures used for in vitro testing of PEDOT electrodes on flexible (polyimide) or rigid MEA substrates. Reproduced according to the terms of the CC BY license.[90] Copyright 2019, the authors, published by Wiley VCH.

hardness, wear resistance, and chemical inertness with a certain level of optical transparency.[85] It was demonstrated to be a promising coating for orthopedic applications with proven tissue tolerance.[86] DLC has been studied as a neural interface electrode from the perspective of biocompatibility. An illustrative example was published by Regan et al., demonstrating that various neural cell types in vitro showed high affinity for DLC electrodes, even allowing patterning of neural networks. These studies were performed with DLC doped with phosphorus (P:DLC), and it was found that cell affinity was further improved by a UV light treatment which caused surface oxidation and caused better cell adherence.[87]

2.1.3. Conducting Polymers

Poly(3,4-ethylenedioxythiophene): Poly(3,4-ethylenedioxythiophene) (PEDOT) has risen to popularity in bioelectronics and has been demonstrated as a promising material for neural interfaces for stimulation and signal recording. It stands out compared to other conducting polymers because it is highly stable in its oxidized p-doped form. It can be prepared by electropolymerization from 3,4-ethylenedioxythiophene solutions, or chemically polymerized. Chemically-polymerized PEDOT with poly(styrene sulfonate) as an polyanionic dopant and colloidal stabilizer, so-called PEDOT:PSS, is an industrial material used since more than 30 years in electrolytic capacitors. Due to its high conductivity, excellent stability, and commercial availability, PEDOT:PSS has been one of the most extensively researched materials in bioelectronics. Moreover, besides the mentioned preparation methods, PEDOT:PSS is commercially available as a solution-processable colloidal dispersion. Dip-coating or spin-coating both are popular methods for PEDOT:PSS deposition. The remarkable feature of conducting polymers, and PEDOT:PSS archetypically, is the presence of mixed electronic–ionic transport (**Figure 7**a). PEDOT:PSS soaks up water from the environment and becomes a hydrogel, capable of conduction of both electronic charges as well as ions. Due to this property, it bridges the ionic–electronic signaling gap which is the essential problem of neural interfaces.[88] Moreover, the entire volume of the PEDOT:PSS electrode can participate in redox reactions and the associated exchange of ions. Therefore the capacitance scales with thickness, making PEDOT:PSS a so-called volumetric capacitor (Figure 7b).[89] In this regard, it is analogous to IrO_x as a pseudofaradaic material which can accommodate extraordinarily high charge injection capacities. Capacitance can be tuned with thickness, and several studies have shown charge injection capacity measurements as a function of thickness and/or electropolymerization charge (this charge corresponds to the total mass of polymer deposited).[90] High interfacial capacitance corresponds also to low impedance values, making PEDOT a competitive choice for recording electrodes. The parameters

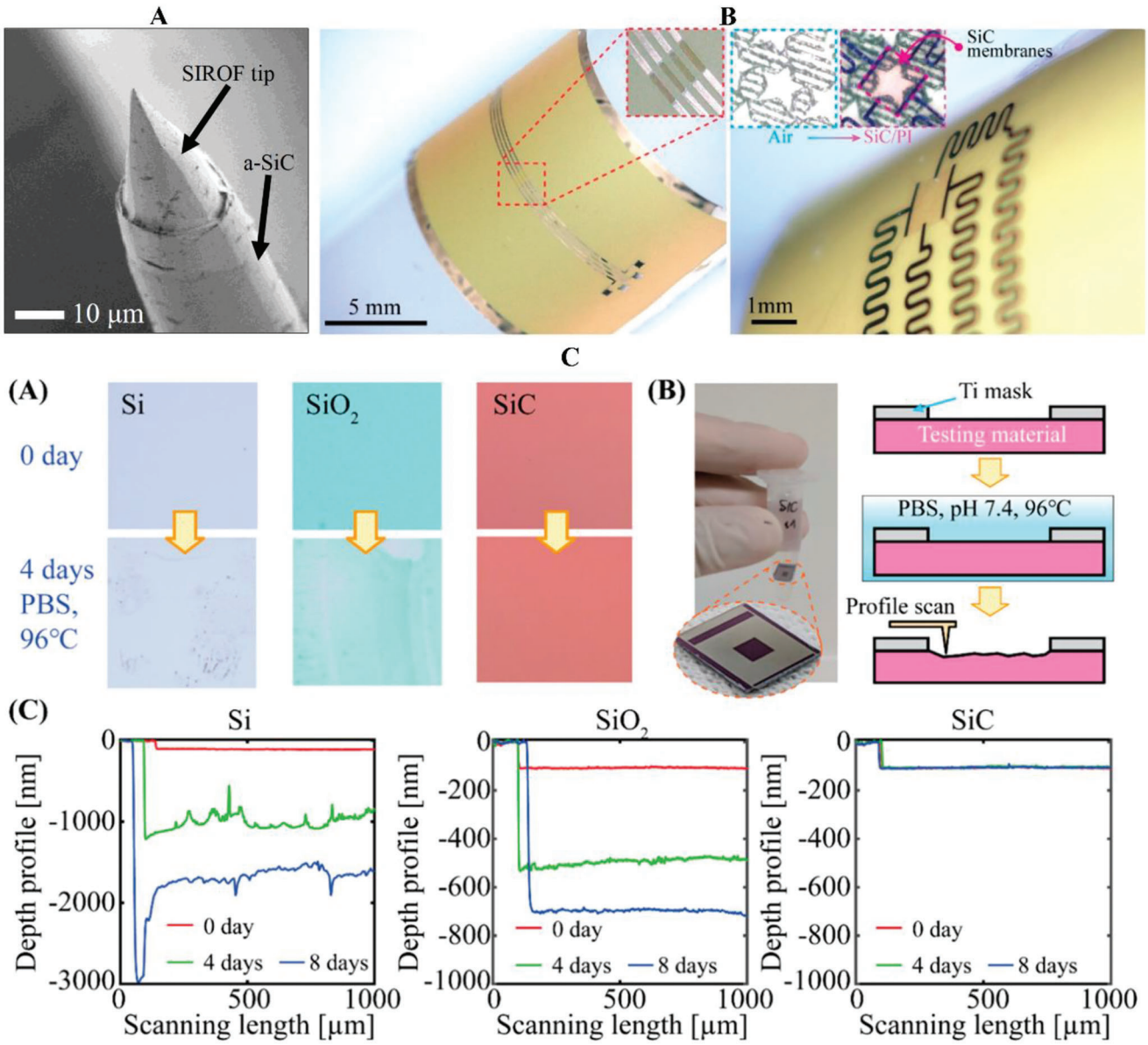

Figure 8. Silicon ceramics. A) Scanning electron microscopy (SEM) image of SIROF (sputtered IrO_x) tip with a-SiC encapsulation layer. These devices were subjected to accelerated lifetime testing and stability was projected to exceed a decade. This figure is reproduced with permission.[117] Copyright 2021, IEEE. B) Flexible SiC on polyimide devices wrapped around a curved surface with diameter of 12 mm. Here, SiC is prepared on a Si wafer at high temperature, and then etched and transferred as a membrane onto the polyimide. This figure is reproduced with permission.[121] Copyright 2019, ACS. C) (A) Colorimetric indication of changes in thickness and/or surface morphology due to hydrolysis from soaking in PBS at pH 7.4 and 96 °C for 4 d. (B) Image of the devices used in determining etching depth by profile scanning. (C) Quantification of the hydrolysis of Si, PECVD oxide, thermal oxide, and SiC.

of PEDOT microelectrodes in the context of neural interfaces has recently been reviewed in detail by Niederhoffer et al.[91] Waafi et al. utilized electrochemically grown PEDOT:PSS on Pt electrodes on stretchable MEAs on PDMS substrates. They determined charge delivery capacitance to be 31 mC cm^{-2} which was approximately two order higher than the CDC of original Pt electrode with the same planar geometry. The value of impedance was 59 kΩ at 1 kHz for electrode with area of 700 μm^2.[59] PEDOT was reported to excel in a comparison of charge injection capacitance versus IrO_x or PtIr, when using constant current stimulation at zero DC voltage bias.[92] There is debate as to where the water window lies with PEDOT.[93] Higher positive potentials can overoxidize and damage PEDOT, while cathodic potentials that can be safely applied appear to be in excess of −1 V versus AgCl.[94] The cathodic water splitting with PEDOT has a high overpotential, at least 1 V overpotential at pH 7. Overoxidation can be used as a patterning method of PEDOT, as photoresist can be used to protect wanted regions of PEDOT while the unwanted regions can be electrochemically or chemically overoxidized and rendered inactive.[95] Despite

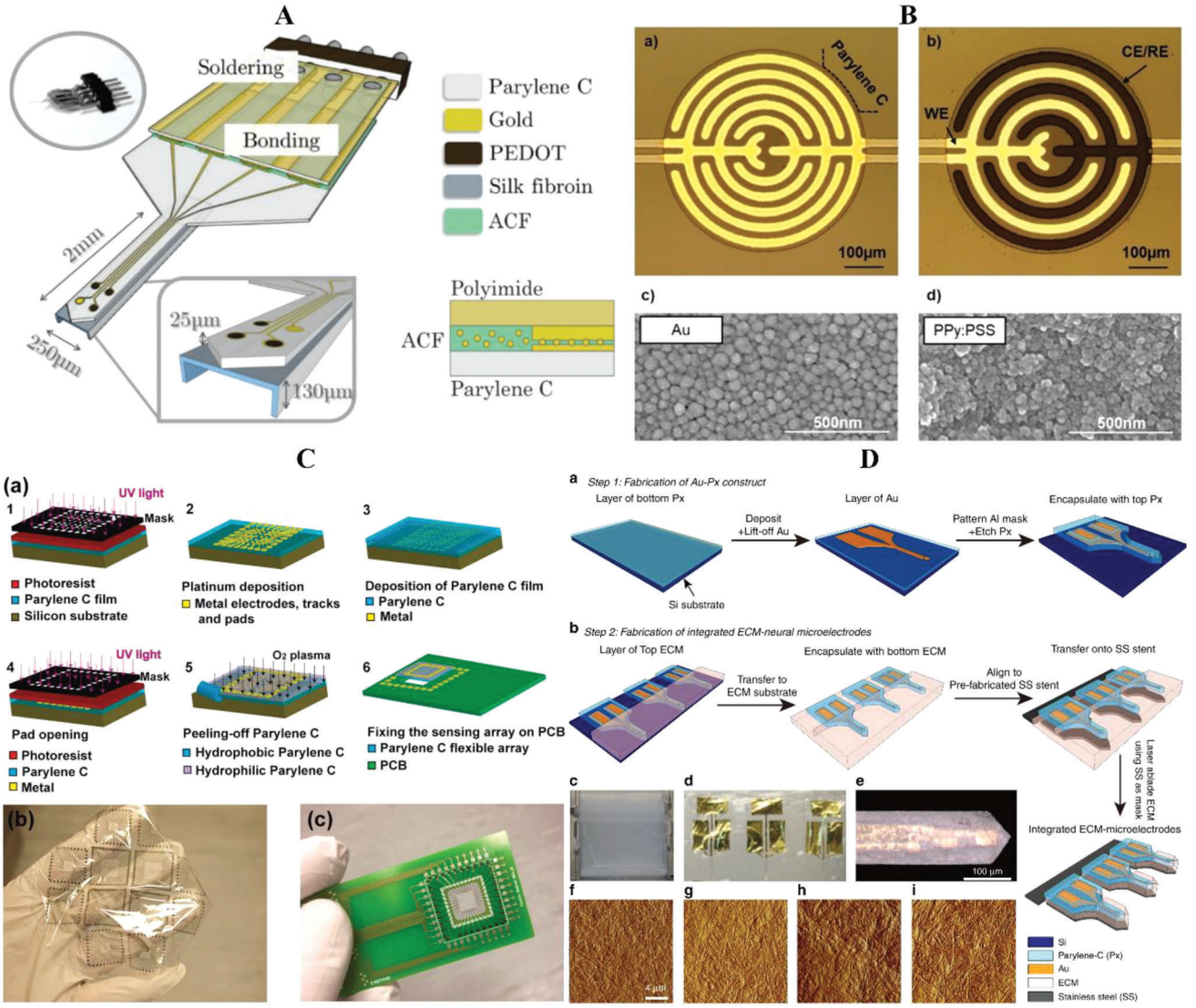

Figure 9. Parylene-C. A) Schematic representation of a complete Parylene-based neural probe consisting of three poly(3,4-ethylenedioxythiophene) (PEDOT)-nanostructured electrodes and one gold electrode as control. The device is bonded using an anisotropic conductive film (ACF) onto a flexible polyimide cable, which is then soldered onto a pin connector adapted to a wireless acquisition system. The cross-section shows bond pads from the device bonded via ACF to the bond pads of the polyimide cable. Reproduced according to the terms of the CC BY license.[125] Copyright 2018, the authors, published by MDPI. B) Microscopy pictures of a) interdigitated gold electrodes with lines and spaces of 20 µm. A thin layer of Parylene C protects the whole chip and is circularly opened to allow access to the sensor area. b) Sensor area consisting of interdigitated electrodes with WE made of gold and CE/RE modified by electrodeposition of PPy:PSS (Q = 170 µC) in brownish color. No color change occurred at the contact leads due to their electrical insulation by Parylene C. c) SEM image of the sputter-deposited gold and d) with PPy:PSS (Q = 170 µC) modified electrode surface, respectively. This figure is reproduced with permission.[126] Copyright 2021, Wiley. C) (a) Schematic of the fabrication process of a flexible sensor; (b) 5 µm-thick Parylene C flexible pH sensing arrays; (c) PCB-based prototype with the flexible chemical array located in the middle. Reproduced according to the terms of the CC BY license.[127] Copyright 2014, the authors, published by MDPI. D) (a) Steps for fabricating an Au/parylene construct, and (b) transfer them onto ECM substrate, integrate with SS stent, and ablate the using excimer laser. Images showing (c) ECM hydrogel (bulk), (d) ECM-microelectrodes, (e) tip and recording sites of an ECM-microelectrode (scale bar: 100 µm); AFM images of ECM substrates: (f) collagen I, (g) collagen I/collagen IV, (h) collagen I/fibronectin, and (i) collagen I/laminin. This figure is reproduced with permission.[128] Copyright 2018, Springer Nature.

excellent indications for performance, long-term chronic in vivo tests with PEDOT are rare. From a mechanical point of view, PEDOT is softer than the other electrode materials mentioned up to now in this review. It has low Young's modulus in units of GPa and is suitable for flexible devices even at higher values of thickness in order of µm.[96]

When applied for recording, neural interface electrodes typically transduce biopotential changes via capacitive coupling, thus converting an input voltage into a voltage signal which is then amplified and digitized. Because of the unique volumetric electrochemistry of PEDOT, in recent years this material inspired a new electrode concept for neural recording: organic

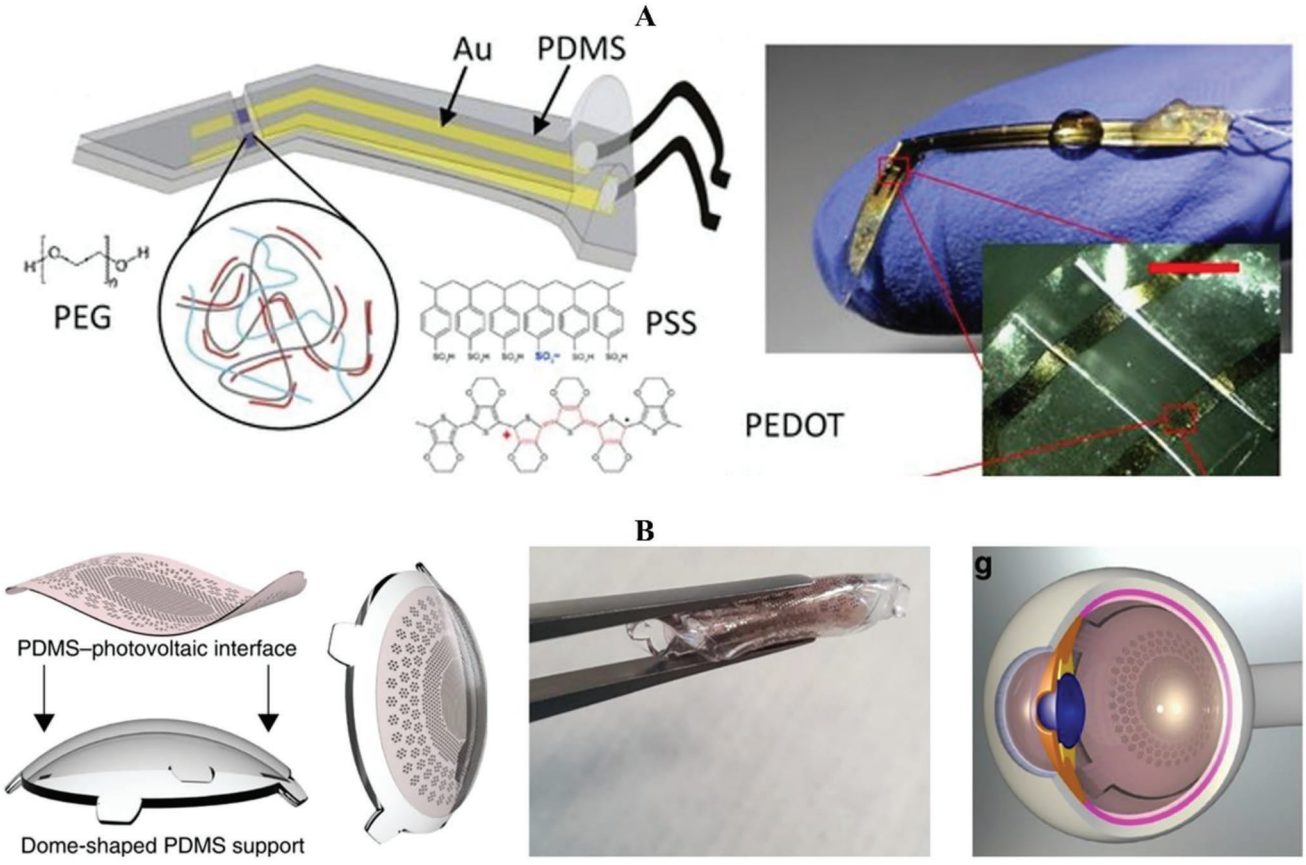

Figure 10. PDMS. A) Stretchable nerve cuff electrode for recording from small peripheral nerves can be enabled by a combination of PDMS, gold conductor lines, and PEDOT-based hydrogels. Reproduced according to the terms of the CC BY license.[135] Copyright 2019, the authors, published by Springer Nature. B) Flexible and foldable retinal stimulation device based on PDMS, the POLYRETINA. Folding allows easy implantation through a small surgical opening in the eye. The device subsequently expands once inside of the eye, representing a unique advantage of using elastomers like PDMS. Reproduced according to the terms of the CC BY license.[137c] Copyright 2018, the authors, published by Springer Nature.

electrochemical transistors (OECTs), or its vertically modified version (VOECTs) with submicron channel length. OECTs can be fabricated into microelectrode pixels which, as transistors, amplify the measured biopotential signal directly at the site of recording. Thus, an input voltage is amplified into an output current, and high gains are possible. This approach can lead to higher signal-to-noise recording when compared to standard PEDOT microelectrodes. While PEDOT-based transistors are several orders slower than inorganic-based transistors, they have high transconductance and still can be modulated at around 1 kHz. Brodsky et al. demonstrated submicron channel length VOECTs with electrochemically grown PEDOT:PF_6 and spin-coated PEDOT:PSS. The highest transconductance (g_m) value of 68 mS was reached for spin-coated PEDOT:PSS. They also determined a cut-off frequency of 1.5 kHz. By using electropolymerized layers, the cutoff could be increased to 3 kHz, but transconductance drops. Balancing high transconductance with bandwidths suitable for high-quality neural recording will determine if OECTs can compete with microelectrodes. Critical comparison of performance of OECT-based neural recording versus microelectrodes is an ongoing topic of study in the field.

Polyaniline: Polyaniline is a material known since the 19th century, and one of the most-studied classic conducting polymers. It is attractive as it is made from extremely low-cost precursors, and it can be easily prepared in a remarkably chemically and chemically stable form. It has two major drawbacks that have prevented its deployment in bioelectronics. First, it is only conductive in acid-doped form. The neutral pH present in physiological conditions will dedope polyaniline and render it essentially insulating.[98] This limits its use as an electrode material. Second, the polymerization process, whether electrochemical or chemical, leads to low-molecular weight byproducts, such as benzidine.[99] Indeed, benzidine and aniline are among the most carcinogenic known organic compounds. There is evidence that toxic low molecular weight byproducts can be completely rinsed from the polyaniline, however the stigma that aniline has in the biomedical community presents a major barrier to exploration and acceptance of polyaniline for such applications. Cytotoxicity studies of "clean" polyaniline films are, unfortunately, indicating of some inherent toxicity, therefore its development in the field remains limited.[100] An intriguing utilization of polyaniline was demonstrated by Liu et al. in form of self-assembled enzymatically-polymerized polyaniline structures in living neural tissues. Low molecular weight precursors are injected together with a redox enzyme, and polyaniline polymerization can be targeted at the cellular level. There is evidence

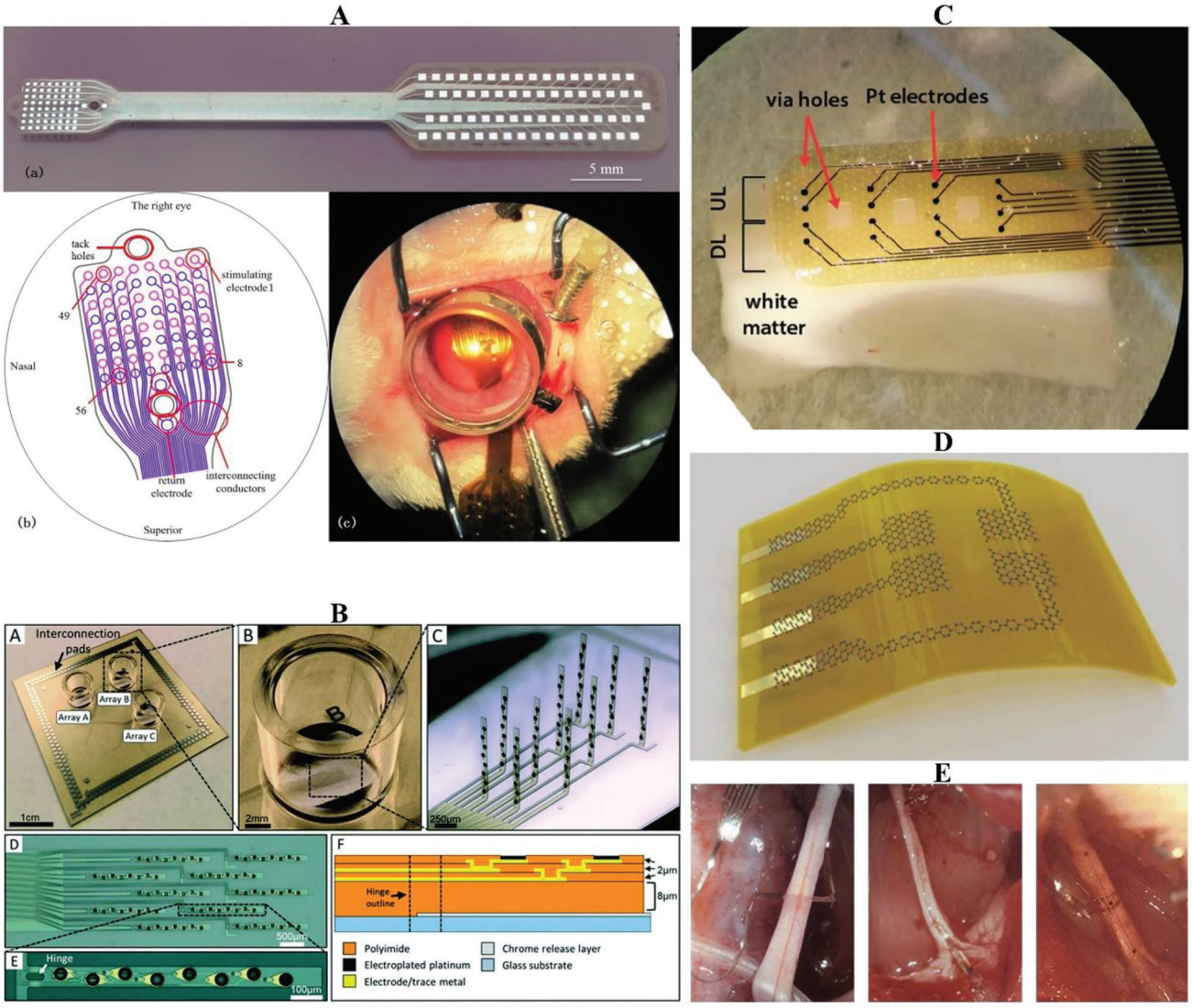

Figure 11. Polyimide. A) Implantable multielectrode array for retinal stimulation experiments in rabbits, based on polyimide as both substrate and encapsulant. Reproduced according to the terms of the CC BY license.[140] Copyright 2013, the authors, published by Springer Nature. B) A 3D MEA for in vitro experiments, utilizing polyimide which is mechanically bent to yield vertical "hinged" multielectrode probes. Reproduced according to the terms of the CC BY license.[141] Copyright 2020, the authors, published by RSC. C) Ultraflexible 8 μm polyimide MEA for both in vitro and in vivo recording experiments. These devices have pores micromachined into them to allow healthy biofluid and gas exchange to the tissues. Reproduced according to the terms of the CC BY license.[141] Copyright 2020, the authors, published by RSC. D) Graphene multielectrode arrays transferred to a commercial 25 μm polyimide foil allow in vivo recording with simultaneous optical imaging, due to the optical transparency of such a MEA. Reproduced according to the terms of the CC BY license.[142] Copyright 2014, Springer Nature. E) Polyimide-based penetrating multichannel electrodes used for transversing peripheral nerves. Reproduced with permission.[143] Copyright 2011, IOP.

that such deposited polyaniline can have (electro)physiological effects on neural tissue, despite the fact that the polyaniline is only in semiconductive form under these conditions.[101] There is interest in expanding this concept of self-assembled conductors in vivo, as evidenced by a recent study on a self-doped polythiophene derivative which can enzymatically polymerize in tissues. Thus, despite attractive properties, polyaniline has yet to find its way into bioelectronics devices of the 2G or 3G type.[102]

Polypyrrole: This conducting polymer was, by virtue of its simple chemistry and facile preparation, the first conducting polymer to be extensively tested in neural interface applications. Cui et al. published a groundbreaking study in 2001 concerning modifying neural microelectrodes with polypyrrole coatings via electropolymerization.[103] The study systematically evaluated the influence of thickness and morphology on capacitance and impedance of electrodes, finding significantly lower impedance than unmodified controls. Polypyrrole shows evidence of having good compatibility with neurons, demonstrating templating/directing effects both with and without application of electrical potential.[104] Polypyrrole possess many similarities with polyaniline, in terms of originating from a simple and low-cost monomer and having a low oxidation potential and thus being

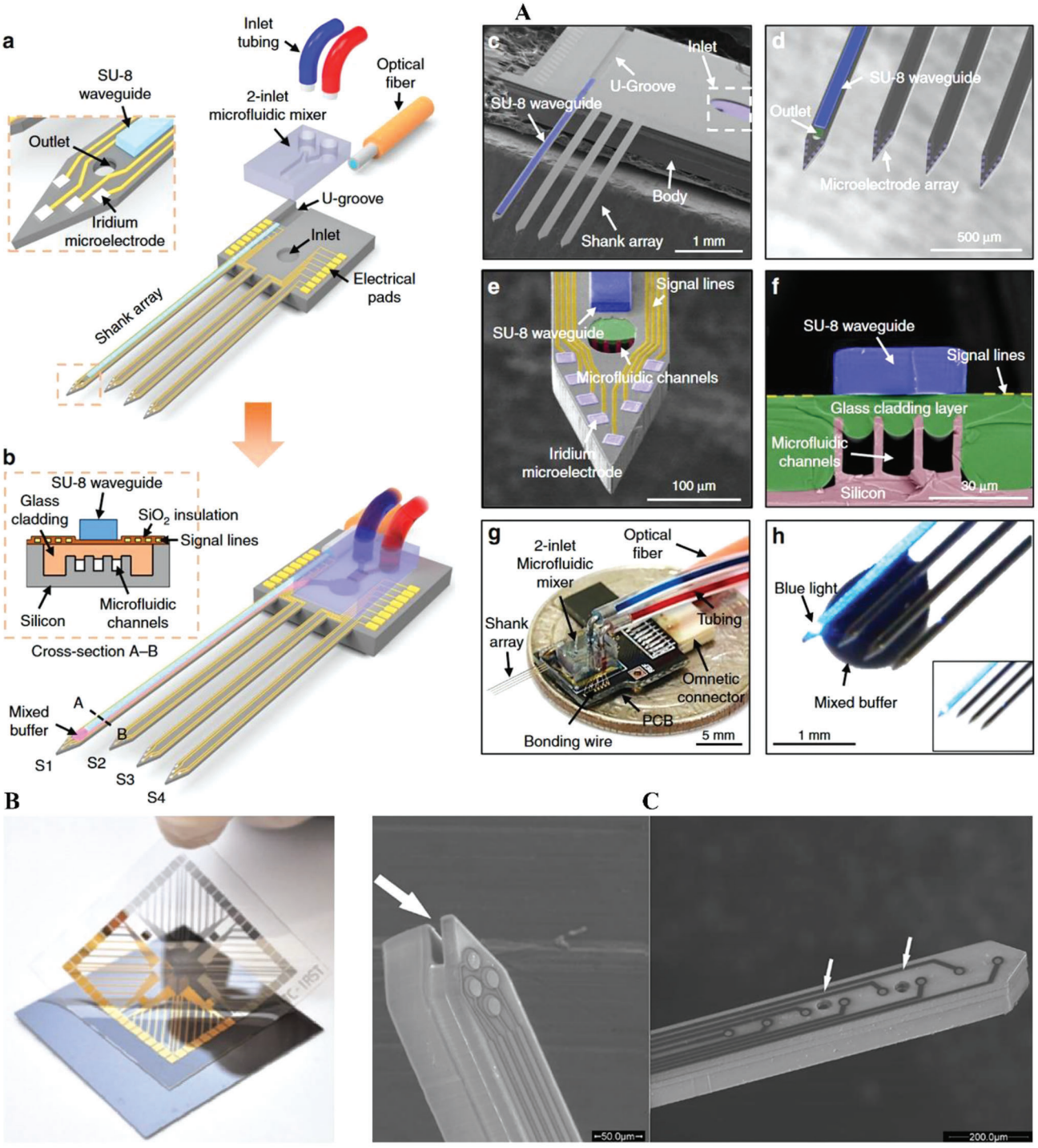

Figure 12. SU-8. A) Multifunctional multishank MEMS neural probe combining microfluidic drug delivery, optical excitation with blue light via a waveguide, and electrophysiological recording. Reproduced according to the terms of the CC BY license.[146] Copyright 2019, the authors, published by Springer Nature. B) Self-standing flexible SU-8-based MEA detached from the Si substrate upon removal of the sacrificial underlayer. Reproduced with permission.[148] Copyright 2011, IOP. C) Penetrating probe with microfluidic drug delivery. Fluidic delivery at the tip, with tetrode configuration (left), and eight-electrode version, with two fluidic outlets in the same face of the probe. The outlets are indicated with arrows (right). Reproduced according to the terms of the CC BY license.[149] Copyright 2015, the authors, published by Frontiers.

easily polymerizable by electrochemical or chemical oxidative routes. However, it has seen much more successful deployment in the neural interface field than polyaniline.[105] Despite its advantages, polypyrrole has been overshadowed by PEDOT in recent years, one reason is that polypyrrole is suffers from degradation of conductivity due to overoxidation, a problem which is less severe with PEDOT.[106]

2.2. Passivation and Encapsulation Materials

Electrical insulation of bioelectronic devices of the 2G and 3G type is a demanding materials science challenge. While 1G devices can make use of "bulk" insulation of plastics and ceramics in the thickness range of hundreds of micrometers up to millimeters, the noninvasivity promised by next-generation thin-film 2G and 3G devices must rely on micrometric or nanometric encapsulation layers. Such encapsulation and passivation layers must maintain excellent electrical insulation without defects, and outstanding (bio)chemical stability with respect to degradation and corrosion. On top of this, they need to be processable in ways that are compatible with existing thin-film device stacks. In particular with flexible 3G devices, low-temperature processes are typically necessary for compatibility with polymeric substrates. Encapsulation layers can be divided into two categories: polymeric plastic materials, and inorganic ceramics materials. Both categories of materials can provide good dielectric strength and insulation, but have important chemical durability distinctions: Inorganic ceramics typically provide a very good barrier to water and to gases, like oxygen. However, they can be easily corroded by aqueous species, like various ions and organic acids/bases. Polymeric materials are, on the other hand, relatively inert with respect to aqueous ions and organic species present in physiological conditions. They are, however, very permeable to oxygen and other gases. It is therefore reasonable to conclude that these two material categories are mutually complementary, and that solutions for long-term chronically implantable bioelectronics most likely must rely on hybrid organic/inorganic encapsulation layers. There are emerging standards in the bioelectronics field for benchmarking the performance of encapsulation layers.[107]

2.2.1. Inorganic Materials

Aluminum Nitride: AlN is semiconductive piezoelectric material with bandgap of ≈6.1 eV well-known from MEMS technology used for fabrication of piezoelectric resonators and transducers such as in cochlear implants or energy harvesters.[108] Furthermore, it is widely used for fabrication of heterojunctions or plasmonic structures.[109] AlN has good indications for use in bioengineering applications, including promising biocompatibility and chemical resistance which were reported in several studies.[110] AlN exhibits high values of hardness which can reach 22 GPa and relatively high Young's modulus of 310 GPa, which is comparable to metallic conductors. Thus, AlN is mechanically robust but still flexible at the nanoscale and microscale. Furthermore, it possesses CMOS compatibility and can be prepared in a wide range of temperatures using many methods from CVD to PVD techniques.[110b,111]

Fabrication into thin film form is quite challenging to obtain all desired parameters such as crystallography and dielectric strength while keeping negligible residual stress. CVD methods usually offer better quality in terms of crystallography and dielectric properties but the preparation requires higher temperatures than in case of PVD techniques.[112] PVD methods such as magnetron sputtering, pulsed laser deposition, or ion-beam sputtering allow preparation of AlN in a temperature range from ambient values up to ≈500 °C.[113] Higher temperature usually means better properties which can be problematic for polymeric substrates or underlayers. Kaufman ion-beam reactive sputtering assisted by secondary ion-beam source allows to prepare excellent quality layers at 330 °C, on the other side, in case of this method, it was proved that layers prepared at 100 °C possess sufficient quality for encapsulation of bioelectronic devices. A combination of AlN with Parylene-C are a promising encapsulation for long-term measurement of MEAs.[71] AlN remains underexplored in the field of bioelectronics.

Silicon Carbide: SiC is a CMOS-compatible material and is under deep investigation because of its wide bandgap (≈3.2 eV) and high temperature stability for high-power electronics with higher durability in comparison to Si.[114] It has low leakage current which makes it more interesting than SOI especially for applications at elevated temperatures.[115] These properties make this material interesting for ICs with mixed signals or photonic applications.[114b] SiC possesses Young's modulus of ≈420 GPa and hardness of ≈30 GPa. Furthermore, it can be prepared in wide range of temperatures from ambient up to more than ≈1500 °C based on the selected CVD or PVD method. It is clear that SiC can vary in parameters like crystallography, mechanical properties, dielectric strength, etc., according to deposition method while the best properties are obtained for epitaxial growth at temperatures usually higher than 1500 °C.[116]

Recently, SiC was used as a passivation layer for neural interfaces due to its chemical and electrochemical resistance. Nguyen et al. replaced parylene-C with amorphous SiC prepared by PECVD at 325 °C for encapsulation of Utah-type penetrating MEAs (**Figure 8**a) and performed accelerated stability tests in PBS which corresponded to ≈22 years in PBS at 37 °C with no recorded electrode failure.[117] A similar experiment with promising results about SiC utilization on MEAs was realized by Deku et al.[118] Further, Cogan et al. performed stability tests of LPCVD SiC and compared the dissolution rate to SiN. They demonstrated zero etch rate of PECVD SiC in PBS at 37 °C while the etch rate of LPCVD SiN was ≈0.4 nm d^{-1}. In addition, they tested SiC deposited on quartz discs in the subcutaneous space of rabbits and did not find inflammatory response.[119] All these mentioned devices were prepared at elevated temperature which is not compatible with flexible substrates with a lower thermal budget like parylene-C. SiC deposition on Parylene-C was mentioned by Bakhshaee et al. using 180 °C for SiC PECVD deposition process, though more study of stability of such structures is necessary.[120]

Silicon Nitride: This material is known from CMOS integrated circuits where it is used as diffusion barrier and passivation layer. Furthermore, it is also employed in MEMS technology as an underlayer, i.e., for membranes. Due to its refractive index of ≈2 it is also interesting in optoelectronics for fabrication of waveguides. Silicon nitride possesses decent biocompatibility,

on the other side the chemical resistance in comparison to AlN is worse making it less suitable for chronic application.[110a,122] Hardness of silicon nitride can reach up to 15 GPa and Young's modulus up to 300 GPa which is quite similar to AlN. Variety of deposition temperatures can be utilized, while in SiN case, the CVD methods are more suitable than PVD because Si is not as reactive as Al, thus, reactive sputtering is not a reliable method. Fabrication is also quite challenging, similarly to preparation of AlN, because of the stoichiometry and residual stress. In the field of flexible bioelectronic devices, where the deposition temperature is the most crucial parameter, PECVD at temperature below 100 °C is a good candidate method.

Silicon Oxide: In general, silicon oxide is used in form of SiO_2 which is one of the oldest materials used in CMOS integrated circuits and MEMS technology. It has been widely used as a passivation layer for substrates and gate electrodes and underlayer for MEMS sensors and actuators. Silicon oxide has ≈3× lower Young's modulus than both AlN and SiN, which makes this material more flexible. Recently, it is used in combination with other materials in multilayer stacks because of the dielectric constant which leads to decreasing performance of semiconductor, thus, it is used only as an extremely thin layer to prevent device from gate leakage currents. Fabrication process can utilize both CVD and PVD methods at broad range of temperatures from ambient (evaporation) up to ≈ 1200 °C (thermal oxidation) which makes it interesting because of its simple preparation. On the other side, it has been proven for many times, that the chemical resistance is poor, thus, it is not possible to use it as neural interface without any other encapsulation material which will create chemical protection. It is important to note that low-temperature silicon oxide has significantly worse insulating properties than a thermally-grown one. Furthermore, SiO_2 has also poor adhesion on noble metals like Au or Pt. Thus, it needs an adhesive interlayer, which introduces an extra step. When exposed to physiological medium, SiO_2 corrodes relatively rapidly, as shown in Figure 8, therefore it cannot be used alone as a passivation solution but must be combined with another encapsulant.

2.2.2. Insulating Polymers

Parylene: Parylene has been one of the most popular enabling substrate and encapsulant materials for 3G devices (**Figure 9**). This polymer is deposited from the vapor phase in a CVD process, to yield an optically transparent, biocompatible, and chemically inert electrical insulating polymeric material. Thicknesses typically range between 1 and 10 µm, though special deposition tools can accomplish thicknesses lower or higher than this range. The CVD process is unique and merits explanation: The di-(*para*-xylene) dimer functions as the precursor, which is sublimated and thermally cracked into reactive monomers in a higher temperature furnace (≈670 °C). The reactive monomers are then transported to the deposition chamber, which is kept at ambient temperature. The final stage of the deposition involves radical polymerization of monomers at the substrate. The biggest advantage of this process is low temperature, which basically allows to deposit parylene on every type of solid material, as well as unrivaled conformability of complex surfaces. The latter is afforded by the fact that the polymerization process occurs in the gaseous phase. The parylene polymer, however, by virtue of its chemical inertness, has poor adhesion to surfaces. The adhesion of parylene can be sponsored by adding a surface treatment with chemical functional groups that can participate in radical polymerization, such as acrylate or methacrylate groups. Thus, the growing parylene polymer attaches to the surface covalently. The methacryloyl silane A174 can be used for attaching parylene to oxide surfaces, while thiol-containing silanes can improve adhesion to gold. Other covalent linkers also have been reported.[123]

Various derivatives of the di-(*para*-xylene) dimer exist, leading to different types of parylenes. The most characterized in the context of bioelectronics is the chlorinated Parylene-C, where each monomer contains a chlorine substituent. This type of Parylene is a good compromise between mechanical and electrical properties, it possesses slightly worse dielectric strength than unsubstituted Parylene-N. On the other side, Parylene-C is mechanically more robust and the gas permeation rate is lower which is more important because the dielectric strength is still extremely high for most of the bioelectronics applications. The most significant concern regarding to Parylene is the conformity of the layer—mechanical defects can behave like pinholes in semiconductor and can dramatically decrease the encapsulation properties which will cause device failure in short time. The next common type is Parylene-F ($C_{16}H_8F_8$) which exhibits poor gas permeability coefficient but it possesses higher thermal resistance than previous types of parylene and is also UV-resistant. Gas permeability may be issue in case of encapsulation when is demanded the protection of device, on the other hand, it can be used as selective membrane for hydrogen or oxygen molecules. It is possible to consider stacking possibilities of different kind of parylene layers to achieve the best properties in terms of encapsulation.[124] Recently, it is also possible to find novel paryleen derivatives such as Parylene-AF4 or Parylene-HT, which contain fluorine. These modified parylenes are thermally resistant and have lower water vapor permeation, and the precursors are more expensive. The better barrier and thermal properties make them interesting candidate materials for bioelectronics, and to the best of our knowledge these types of parylenes have not been reported in these applications yet.

Polydimethylsiloxane: Polydimethylsiloxane (PDMS) is an elastomeric material which is ubiquitous as insulation in 1G devices. It is chemically inert, soft, and flexible (modulus 1–3 MPa), and has a strong track record as a biocompatible and safe material.[129] In 1G devices, it is deployed as an encapsulant at thicknesses typically in excess of 100 µm. It is a crosslinked polymeric material which is processed by mixing a PDMS base polymer together with a cross-linker. The material hardens by crosslinking, the curing speed of which is determined by the temperature, from room temperature up to around 150°.[130] Curing conditions also determine the mechanical properties of PDMS. Before it is cured, it can be spin coated or dip-coated onto substrates. Thinner films can be achieved by diluting the PDMS with a suitable organic solvent. Using these techniques, PDMS can be incorporated into 2G and 3G thin film devices. Microfabrication is complicated however as etching is difficult due to its chemical inertness and mechanical softness.[131] Its low surface energy is problematic for adhesion of deposited metal

layers. This problem can be partly solved by chemical treatment or by thermal bonding when the PDMS is deposited on metallic layers. Such processing is often not compatible with fabrication of more sophisticated devices requiring several fabrication steps.[132] Next option of adhesion improvement is deposition of adhesion layer like Ti using high-energetic deposition method such as high-power impulse magnetron sputtering.[133] PDMS can withstand relatively high temperatures. The decomposition starts in the range from 300 to 400 °C, depending on the environment.[134] An advantage is its simple preparation on wafers which can be realized by precursor spin-coating followed by curing in wide range of temperatures up to 150 °C. Despite its complications with microfabrication compatibility, it is widely used as a substrate and encapsulant for next-generation bioelectronics, such as MEAs for brain and peripheral nerve interfaces. PDMS can be used to make microscaled cuff electrodes for nerve recording, which not only are flexible but also stretchable (**Figure 10**a).[135] PDMS is widely used in microfluidics, and this knowledge was repurposed to make nerve microconduits for regenerative peripheral interface, demonstrated on the sciatic nerve.[136] The highly flexible nature of PDMS is showcased in the application of implantable MEAs for retinal stimulation.[137] In these devices, PDMS is used for both substrate and encapsulation to make a foldable implant which can be inserted through a small surgical opening in the eye and then unfurled once inside (Figure 10b).[137c]

Polyimides: Polyimides are a type of engineering plastic known for high thermal and chemical stability. They contain imide groups ($-R_1CO-NR_2-COR_3-$) in the polymer backbone.[138]

Polyimides are mostly known from the field of printed circuit board (PCB) technology. Flexible substrates for circuits containing surface mount devices or interconnections of devices in form of flex cables rely on polyimides. Furthermore, it is also well-known from the field of PCB repair, when it is used in the form of Kapton tape to protect covered devices from outer heat sources during repairs. From the point of view of 3G bioelectronics, polyimides have a significantly higher temperature tolerance than competing materials like parylene-C or PDMS. This enables compatibility with a wider range of fabrication and etching processes. Polyimides have relatively low Young's modulus in units of GPa, and is also reported to be well-tolerated by tissue during chronic implantation.[139] They possess excellent insulation properties especially with thickness above 1 µm. Contrary to the Parylene deposition, which is simple and highly conformal process, polyimide require handling by solution deposition from precursor polymers. These are usually spin-coated and heated to temperatures around 200 °C or even around 300 °C to create the highly stable imide linkages required to form the target polymer. This annealing process must be very careful controlled in terms of temperature ramp and proper atmosphere, and usually takes several hours.[138] This annealing processing step makes polyimides sometimes inapplicable as encapsulation layer when devices contain sensitive components, such as gold layers. Thus, a popular approach is to use polyimide as the device substrate, while using parylene-C as the encapsulant. **Figure 11** shows a range of MEA applications based on polyimide, either for in vitro or in vivo electrophysiology.

SU-8 photoresist: SU-8 is negative epoxy-based photoresist (PR) which is often employed as a first-choice encapsulation layer because of its easy preparation and high-aspect ratio shape definition using a straightforward UV lithography process. It consists of a polyphenolic (aka Novolac) backbone modified with epoxide functional groups, solvent, and photoacid generator. Important advantage is the possibility to prepare SU-8 with thickness in the range from nanometers up to hundreds of µm based on the specific commercial formulation of the resin. As a crosslinked epoxy material, the Young's modulus is usually in range from 2 to 5 GPa.[144] There is no unified statement about its full biocompatibility, especially for in vivo applications. However, it is possible to perform surface modifications with oxygen plasma treatment or grafting of biocompatible polymers to reduce biofouling.[145] For example, the SU-8 was studied for encapsulation of MEAs for extracellular recording of neurons of rat hippocampus which were cultured on this device. They compared this device to one encapsulated with SiN layer and confirmed stable impedance for three weeks, comparable to a "control" sample using SiN encapsulation.[48b] It is important to note, that SU-8 is also famous because of its optical properties and can be used as optical waveguide. Shin et al. fabricated multifunctional multi-shank neural probes employing SU-8 optical waveguides (**Figure 12**) and investigated their performance in vivo. They reported that probes caused little immune response over two weeks.[146] Luan et al. used SU-8 for preparation of highly flexible nanoelectronic thread electrodes with subcellular dimensions. They performed in vivo tests of implants in rats for four months and proved excellent stability and reliability during whole period of device stressing.[147] These are among the thinnest probes ever implanted, and such a long in vivo stability result is encouraging.

3. Conclusion

Bioelectronic devices, both for enabling basic research and novel therapeutics, is a field that places high demands on advanced electronic materials. The list of conditions materials must meet for electronic performance, stability, and safety is extensive and greatly exceeds that is normally expected for consumer electronics and many other engineering applications. For conducting electronic materials, key properties for interconnects are high conductivity, ease of processability, and reliability/stability. For neural interface electrodes, conductivity does not need to be high, but interfacial impedance must be minimized and demands on stability are paramount. At present, there is no ideal material for either of these applications, always there are trade-offs to consider. Often, a practical resolution cab be found in a judicious combination of two or more materials, for instance gold with adhesion layers as an interconnect, and a conducting polymer like PEDOT as the interface electrode. On the side of encapsulation, limitations exist as well. Neither ceramic nor polymeric materials along fulfill necessary barrier properties for water vapor and ions while combining resistance to corrosion. Here to a hybrid solution of two or more materials is the way forward. An example can be parylene-C as a polymeric barrier to ions and corrosive reactions, with a ceramic nitride layer to block water vapor/gas permeability. In terms of actual applications outside of basic research, the 2G and 3G devices discussed in this review have yet

to compete with bulky 1G devices on a large scale. This is mostly due to issues of safety and reliability. While the amount of scientific papers disclosing advanced new materials and devices for bioelectronics continues to grow, there is an increasing realization in the community that it is time to move on from "proof-of-concept" level demonstrations and invest time and effort into studying materials and devices from the stability, safety, and reliability standpoint. This review has been aimed to provide an introduction to materials and concepts in the thin film field, with attention to practical advantages as well as challenges.

Acknowledgements

This work was supported by the European Research Council (ERC) under the European Union's Horizon 2020 research and innovation program (E.D.G. Grant Agreement No. 949191), by the Grant Agency of the Czech Republic under Contract No. 23-07432S, and by funding from the National Center for Neurological Research, supported by the Czech Ministry of Education, Youth, and Sports (LX22NPO5107).

Conflict of Interest

The authors declare no conflict of interest.

Keywords

bioelectronics, biomedical engineering, encapsulation, functional materials, thin films

Received: April 18, 2023
Revised: May 31, 2023
Published online: July 9, 2023

[1] a) I. Willner, E. Katz, *Bioelectronics*, Wiley-VCH, Weinheim **2005**; b) M. Berggren, E. D. Głowacki, D. T. Simon, E. Stavrinidou, K. Tybrandt, *Chem. Rev.* **2022**, *122*, 4826; c) E. Katz, *Implantable Bioelectronics*, Wiley-VCH, Weinheim **2014**; d) *Handbook of Bioelectronics: Directly Interfacing Electronics and Biological Systems*, Cambridge University Press, Cambridge **2015**.
[2] a) C. J. Bettinger, M. Ecker, T. D. Y. Kozai, G. G. Malliaras, E. Meng, W. Voit, *MRS Bull.* **2020**, *45*, 655; b) R. Chen, A. Canales, P. Anikeeva, *Nat. Rev. Mater.* **2017**, *2*, 16093.
[3] C. E. Larson, E. Meng, *J. Neurosci. Methods* **2020**, *332*, 108523.
[4] a) S. F. Cogan, *Annu. Rev. Biomed. Eng.* **2008**, *10*, 275; b) J. Lipus, K. Krukiewicz, *Measurement* **2022**, *191*, 110822.
[5] J. Maeng, B. Chakraborty, N. Geramifard, T. Kang, R. T. Rihani, A. Joshi-Imre, S. F. Cogan, *J. Biomed. Mater. Res., Part B* **2020**, *108*, 880.
[6] M. Ganji, A. Tanaka, V. Gilja, E. Halgren, S. Dayeh, *Adv. Funct. Mater.* **2017**, *27*, 1703019.
[7] R. Kim, N. Hong, Y. Nam, *Biotechnol. J.* **2013**, *8*, 206.
[8] H. Cui, X. Xie, S. Xu, L. L. H. Chan, Y. Hu, *Biomed. Eng. Online* **2019**, *18*, 86.
[9] S. F. Cogan, T. D. Plante, J. Ehrlich, in *Conf. Proc. Annual Int. Conf. IEEE Engineering in Medicine and Biology Society*, vol. *2004*, IEEE **2004**, p. 4153.
[10] F. Deku, A. Joshi-Imre, A. Mertiri, T. J. Gardner, S. F. Cogan, *J. Electrochem. Soc.* **2018**, *165*, D375.
[11] Q. Zeng, S. Yu, Z. Fan, Y. Huang, B. Song, T. Zhou, *Nanomaterials* **2022**, *12*, 3445.
[12] X. Y. Kang, J. Q. Liu, H. C. Tian, B. Yang, Y. NuLi, C. S. Yang, in *Annual Int. Conf. IEEE Engineering in Medicine and Biology Society*, Vol. *2014*, IEEE **2014**, p. 478.
[13] G. Ganske, E. Slavcheva, A. van Ooyen, W. Mokwa, U. Schnakenberg, *Thin Solid Films* **2011**, *519*, 3965.
[14] L. Li, C. Jiang, W. Duan, Z. Wang, F. Zhang, C. He, T. Long, L. Li, *Microsyst. Nanoeng.* **2022**, *8*, 96.
[15] R. T. Leung, M. N. Shivdasani, D. A. X. Nayagam, R. K. Shepherd, *IEEE Trans. Biomed. Eng.* **2015**, *62*, 849.
[16] A. N. Ivanovskaya, A. M. Belle, A. M. Yorita, F. Qian, S. Chen, A. Tooker, R. G. Lozada, D. Dahlquist, V. Tolosa, *J. Electrochem. Soc.* **2018**, *165*, G3125.
[17] J. D. Weiland, D. J. Anderson, M. S. Humayun, *IEEE Trans. Biomed. Eng.* **2002**, *49*, 1574.
[18] J. Arpa, K. Rechendorff, P. S. Wismayer, B. Mallia, *Mater. Chem. Phys.* **2022**, *289*, 126435.
[19] M. Patan, T. Shah, M. Sahin, in *Conf. Proc.: Annual Int. Conf. IEEE Engineering in Medicine and Biology Society*, Vol. *2006*, IEEE, **2006**, p. 890.
[20] A. Cisnal, F. R. Ihmig, J.-C. Fraile, J. Pérez-Turiel, V. Muñoz-Martinez, *Sensors* **2019**, *19*, 2725.
[21] A. A. Silva, R. A. Pinheiro, C. D. A. Razzino, A. Contin, E. J. Corat, *MRS Adv.* **2017**, *2*, 2247.
[22] S. Nimbalkar, E. Castagnola, A. Balasubramani, A. Scarpellini, S. Samejima, A. Khorasani, A. Boissenin, S. Thongpang, C. Moritz, S. Kassegne, *Sci. Rep.* **2018**, *8*, 6958.
[23] S. Wilks, S. Richardson-Burn, J. Hendricks, D. Martin, K. Otto, *Front. Neuroeng.* **2009**, *2*, 7.
[24] A. S. Pranti, A. Schander, A. Bödecker, W. Lang, *Sens. Actuators, B* **2018**, *275*, 382.
[25] B. Lu, H. Yuk, S. Lin, N. Jian, K. Qu, J. Xu, X. Zhao, *Nat. Commun.* **2019**, *10*, 1043.
[26] M. Skorupa, D. Więcławska, D. Czerwińska-Główka, M. Skonieczna, K. Krukiewicz, *Polymers* **2021**, *13*, 1948.
[27] Y. Lu, T. Li, X. Zhao, M. Li, Y. Cao, H. Yang, Y. Y. Duan, *Biomaterials* **2010**, *31*, 5169.
[28] a) L. Aldous, D. S. Silvester, C. Villagrán, W. R. Pitner, R. G. Compton, M. C. Lagunas, C. Hardacre, *New J. Chem.* **2006**, *30*, 1576; b) S. Cherevko, A. A. Topalov, A. R. Zeradjanin, I. Katsounaros, K. J. J. Mayrhofer, *RSC Adv.* **2013**, *3*, 16516.
[29] A. Ignaczak, E. Santos, W. Schmickler, *Curr. Opin. Electrochem.* **2019**, *13*, 140.
[30] a) D. R. Merrill, M. Bikson, J. G. Jefferys, *J. Neurosci. Methods* **2005**, *141*, 171; b) S. L. Morton, M. Daroux, J. T. Mortimer, presented at *Proc. Annual Int. Conf. IEEE Engineering in Medicine and Biology Society*, Volume *13*, October–November, **1991**; c) J. Ehlich, L. Migliaccio, I. Sahalianov, M. Nikić, J. Brodský, I. Gablech, X. T. Vu, S. Ingebrandt, E. D. Głowacki, *J. Neural Eng.* **2022**, *19*, 036045.
[31] M. Gryszel, E. D. Głowacki, *Chem. Commun.* **2020**, *56*, 1705.
[32] C. Hassler, R. P. von Metzen, P. Ruther, T. Stieglitz, *J. Biomed. Mater. Res., Part B* **2010**, *93*, 266.
[33] K. Leosson, A. S. Ingason, B. Agnarsson, A. Kossoy, S. Olafsson, M. C. Gather, *Nanophotonics* **2013**, *2*, 3.
[34] M. Silverå Ejneby, M. Jakešová, J. J. Ferrero, L. Migliaccio, I. Sahalianov, Z. Zhao, M. Berggren, D. Khodagholy, V. Đerek, J. N. Gelinas, E. D. Głowacki, *Nat. Biomed. Eng.* **2022**, *6*, 741.
[35] T. Araki, F. Yoshida, T. Uemura, Y. Noda, S. Yoshimoto, T. Kaiju, T. Suzuki, H. Hamanaka, K. Baba, H. Hayakawa, T. Yabumoto, H. Mochizuki, S. Kobayashi, M. Tanaka, M. Hirata, T. Sekitani, *Adv. Healthcare Mater.* **2019**, *8*, 1900130.
[36] Y. H. Cheng, S. J. Liu, J. H. Jiang, *Talanta* **2021**, *222*, 121536.
[37] C. A. Goss, D. H. Charych, M. Majda, *Anal. Chem.* **1991**, *63*, 85.
[38] G. Wang, X. He, L. Wang, A. Gu, Y. Huang, B. Fang, B. Geng, X. Zhang, *Microchim. Acta* **2012**, *180*, 161.

[39] M. Eickenscheidt, E. Singler, T. Stieglitz, *Polym. J.* **2019**, *51*, 1029.
[40] P. R. F. Rocha, P. Schlett, U. Kintzel, V. Mailänder, L. K. J. Vandamme, G. Zeck, H. L. Gomes, F. Biscarini, D. M. de Leeuw, *Sci. Rep.* **2016**, *6*, 34843.
[41] a) T. L. Rose, E. M. Kelliher, L. S. Robblee, *J. Neurosci. Methods* **1985**, *12*, 181; b) I. Schoen, P. Fromherz, *Biophys. J.* **2007**, *92*, 1096.
[42] a) W. Banerjee, A. Kashir, S. Kamba, *Small* **2022**, *18*, 2107575; b) J. Müller, P. Polakowski, S. Mueller, T. Mikolajick, *ECS J. Solid State Sci. Technol.* **2015**, *4*, N30.
[43] M. T. Becker, *AIP Adv.* **2021**, *11*, 065106.
[44] a) S. Klamklang, H. Vergnes, F. Senocq, K. Pruksathorn, P. Duverneuil, S. Damronglerd, *J. Appl. Electrochem.* **2009**, *40*, 997; b) P. Yin, Y. Liu, L. Xiao, C. Zhang, *Polymers* **2021**, *13*, 2834. c) J. Hämäläinen, M. Kemell, F. Munnik, U. Kreissig, M. Ritala, M. Leskelä, *Chem. Mater.* **2008**, *20*, 2903; d) E. N. El Sawy, V. I. Birss, *J. Mater. Chem.* **2009**, *19*, 8244.
[45] C. Chen, S. Ruan, X. Bai, C. Lin, C. Xie, I.-S. Lee, *Mater. Sci. Eng., C* **2019**, *103*, 109865.
[46] I.-S. Lee, C.-N. Whang, K. Choi, M.-S. Choo, Y.-H. Lee, *Biomaterials* **2002**, *23*, 2375.
[47] S. Gawad, M. Giugliano, M. Heuschkel, B. Wessling, H. Markram, U. Schnakenberg, P. Renaud, H. Morgan, *Front. Neuroeng.* **2009**, *2*, 1.
[48] a) S. A. M. Marzouk, S. Ufer, R. P. Buck, T. A. Johnson, L. A. Dunlap, W. E. Cascio, *Anal. Chem.* **1998**, *70*, 5054; b) H. Jeong, S. Hwang, K. Min, S. B. Jun, *Micromachines* **2021**, *12*, 1347.
[49] G. Topalov, G. Ganske, E. Lefterova, U. Schnakenberg, E. Slavcheva, *Int. J. Hydrogen Energy* **2011**, *36*, 15437.
[50] B.-Y. Wang, Z. C. Chen, M. Bhuckory, T. Huang, A. Shin, V. Zuckerman, E. Ho, E. Rosenfeld, L. Galambos, T. Kamins, K. Mathieson, D. Palanker, *Nat. Commun.* **2022**, *13*, 6627.
[51] S. F. Cogan, J. Ehrlich, T. D. Plante, M. D. Gingerich, D. B. Shire, *IEEE Trans. Biomed. Eng.* **2010**, *57*, 2313.
[52] Z. C. Lin, C. Xie, Y. Osakada, Y. Cui, B. Cui, *Nat. Commun.* **2014**, *5*, 3206.
[53] B. Ji, Z. Guo, M. Wang, B. Yang, X. Wang, W. Li, J. Liu, *Microsyst. Nanoeng.* **2018**, *4*, 27.
[54] J. Wrbanek, K. Laster, *NASA/TM* **2005**, https://ntrs.nasa.gov/citations/20050061011.
[55] a) J. S. Agustsson, U. B. Arnalds, A. S. Ingason, K. B. Gylfason, K. Johnsen, S. Olafsson, J. T. Gudmundsson, presented at *17th Int. Vacuum Congress/13th Int. Conf. Surface Science/Int. Conf. Nanoscience and Technology*, Stockholm, Sweden, July **2007**; b) F. Purkl, T. English, G. Yama, J. Provine, A. K. Samarao, A. Feyh, G. O. Brien, O. Ambacher, R. T. Howe, T. W. Kenny, presented at *2013 IEEE 26th Int. Conf. Micro Electro Mechanical Systems (MEMS)*, January **2013**; c) O. Valet, P. Doppelt, P. Baumann, M. Schumacher, E. Balnois, F. Bonnet, H. Guillon, *Microelectron. Eng.* **2002**, *64*, 457.
[56] R. A. Green, P. B. Matteucci, C. W. D. Dodds, J. Palmer, W. F. Dueck, R. T. Hassarati, P. J. Byrnes-Preston, N. H. Lovell, G. J. Suaning, *J. Neural Eng.* **2014**, *11*, 056017.
[57] M. Gryszel, M. Jakešová, T. Lednický, E. D. Głowacki, *Adv. Mater. Interfaces* **2022**, *9*, 2101973.
[58] a) L. Rivas, S. Dulay, S. Miserere, L. Pla, S. B. Marin, J. Parra, E. Eixarch, E. Gratacós, M. Illa, M. Mir, J. Samitier, *Biosens. Bioelectron.* **2020**, *153*, 112028; b) R. T. Leung, M. N. Shivdasani, D. A. Nayagam, R. K. Shepherd, *IEEE Trans. Biomed. Eng.* **2015**, *62*, 849; c) Z. Miripour, P. Aghaee, R. Mahdavi, M. A. Khayamian, A. Mamdouh, M. R. Esmailinejad, S. Mehrvarz, N. Yousefpour, N. Namdar, M. Mousavi-kiasary, A. Vajhi, F. Abbasvandi, P. Hoseinpour, H. Ghafari, M. Abdolahad, *Nanoscale* **2020**, *12*, 22129.
[59] C. Boehler, D. M. Vieira, U. Egert, M. Asplund, *ACS Appl. Mater. Interfaces* **2020**, *12*, 14855.
[60] F. L. Gielen, P. Bergveld, *Med. Biol. Eng. Comput.* **1982**, *20*, 77.
[61] I. R. Cassar, C. Yu, J. Sambangi, C. D. Lee, J. J. Whalen, A. Petrossians, W. M. Grill, *Biomaterials* **2019**, *205*, 120.
[62] E. della Valle, B. Koo, P. R. Patel, Q. Whitsitt, E. K. Purcell, C. A. Chestek, J. D. Weiland, *Front. Nanotechnol.* **2021**, *3*,782883.
[63] M. Schaldach, M. Hubmann, A. Weikl, R. Hardt, *Pacing Clin. Electrophysiol.* **1990**, *13*, 1891.
[64] U. Egert, B. Schlosshauer, S. Fennrich, W. Nisch, M. Fejtl, T. Knott, T. Müller, H. Hämmerle, *Brain Res. Brain Res. Protoc.* **1998**, *2*, 229.
[65] L. A. Cyster, D. M. Grant, K. G. Parker, T. L. Parker, *Biomol. Eng.* **2002**, *19*, 171.
[66] S. Meijs, M. Fjorback, C. Jensen, S. Sørensen, K. Rechendorff, N. J. Rijkhoff, *Front. Neurosci.* **2015**, *9*, 268.
[67] N. A. Steinmetz, C. Aydin, A. Lebedeva, M. Okun, M. Pachitariu, M. Bauza, M. Beau, J. Bhagat, C. Böhm, M. Broux, S. Chen, J. Colonell, R. J. Gardner, B. Karsh, F. Kloosterman, D. Kostadinov, C. Mora-Lopez, J. O'Callaghan, J. Park, J. Putzeys, B. Sauerbrei, R. J. J. van Daal, A. Z. Vollan, S. Wang, M. Welkenhuysen, Z. Ye, J. T. Dudman, B. Dutta, A. W. Hantman, K. D. Harris, et al., *Science* **2021**, *372*, 258.
[68] a) F. Elstner, A. Ehrlich, H. Giegengack, H. Kupfer, F. Richter, *J. Vac. Sci. Technol., A* **1994**, *12*, 476; b) P. Saikia, A. Joseph, R. Rane, B. K. Saikia, S. Mukherjee, *Philos. Mag.* **2013**, *7*, 66; c) V. A. Burdovitsin, D. A. Golosov, E. M. Oks, A. V. Tyunkov, Y. G. Yushkov, D. B. Zolotukhin, S. M. Zavadsky, *Surf. Coat. Technol.* **2019**, *358*, 726.
[69] U. Egert, B. Schlosshauer, S. Fennrich, W. Nisch, M. Fejtl, T. Knott, T. Müller, H. Hämmerle, *Brain Res. Protoc.* **1998**, *2*, 229.
[70] B. Dutta, A. Andrei, T. D. Harris, C. M. Lopez, J. O'Callahan, J. Putzeys, B. C. Raducanu, S. Severi, S. D. Stavisky, E. M. Trautmann, M. Welkenhuysen, K. V. Shenoy, presented at *2019 IEEE Int. Electron Devices Meeting (IEDM)*, December **2019**.
[71] I. Gablech, L. Migliaccio, J. Brodský, M. Havlíček, P. Podešva, R. Hrdý, J. Ehlich, M. Gryszel, E. D. Głowacki, *Adv. Electron. Mater.* **2023**, *9*, 2200980.
[72] a) E. Patrick, M. E. Orazem, J. C. Sanchez, T. Nishida, *J. Neurosci. Methods* **2011**, *198*, 158; b) A. S. Idil, N. Donaldson, *J. Neural Eng.* **2018**, *15*, 021006.
[73] R. Li, L. Wang, D. Kong, L. Yin, *Bioact. Mater.* **2018**, *3*, 322.
[74] L. Yin, H. Cheng, S. Mao, R. Haasch, Y. Liu, X. Xie, S.-W. Hwang, H. Jain, S.-K. Kang, Y. Su, R. Li, Y. Huang, J. A. Rogers, *Adv. Funct. Mater.* **2014**, *24*, 645.
[75] a) J. Wu, X. Liu, L. Yan, L. Zhang, *Mater. Lett.* **2017**, *196*, 414; b) X. Sun, J. Fan, C. Fu, L. Yao, S. Zhao, J. Wang, J. Xiao, *Sci. Rep.* **2017**, *7*, 10290.
[76] a) Z. Deng, Y. Gong, Y. Luo, Y. Tian, *Biosens. Bioelectron.* **2009**, *24*, 2465; b) L. Santos, C. Silveira, E. Elamurugu, J. Neto, D. Nunes, L. Pereira, R. Martins, J. Viegas, J. Moura, S. Todorovic, M. G. Almeida, E. Fortunato, *Sens. Actuators, B* **2015**, *223*, 186.
[77] a) M. D. Dickey, *ACS Appl. Mater. Interfaces* **2014**, *6*, 18369; b) M. D. Dickey, *Adv. Mater.* **2017**, *29*, 1606425; c) F.-M. Allioux, M. B. Ghasemian, W. Xie, A. P. O'Mullane, T. Daeneke, M. D. Dickey, K. Kalantar-Zadeh, *Nanoscale Horiz.* **2022**, *7*, 141.
[78] N. Hallfors, A. Khan, M. D. Dickey, A. M. Taylor, *Lab Chip* **2013**, *13*, 522.
[79] T. Latif, M. McKnight, M. D. Dickey, A. Bozkurt, *PLoS One* **2018**, *13*, e0203880.
[80] S. Chen, R. Zhao, X. Sun, H. Wang, L. Li, J. Liu, *Adv. Healthcare Mater.* **2023**, *12*, 2201924.
[81] M. Devi, M. Vomero, E. Fuhrer, E. Castagnola, C. Gueli, S. Nimbalkar, M. Hirabayashi, S. Kassegne, T. Stieglitz, S. Sharma, *J. Neural Eng.* **2021**, *18*, 041007.
[82] E. Kaivosoja, S. Sainio, J. Lyytinen, T. Palomäki, T. Laurila, S. I. Kim, J. G. Han, J. Koskinen, *Surf. Coat. Technol.* **2014**, *259*, 33.
[83] M. Bramini, G. Alberini, E. Colombo, M. Chiacchiaretta, M. L. DiFrancesco, J. F. Maya-Vetencourt, L. Maragliano, F. Benfenati, F. Cesca, *Front. Syst. Neurosci.* **2018**, *12*, 12.

[84] S. W. Shaner, M. Islam, M. B. Kristoffersen, R. Azmi, S. Heissler, M. Ortiz-Catalan, J. G. Korvink, M. Asplund, *Biosens. Bioelectron. X* **2022**, *11*, 100143.
[85] J. Robertson, *Mater. Sci. Eng., R* **2002**, *37*, 129.
[86] M. Allen, B. Myer, N. Rushton, *J. Biomed. Mater. Res.* **2001**, *58*, 319.
[87] E. M. Regan, J. B. Uney, A. D. Dick, Y. Zhang, J. Nunez-Yanez, J. P. McGeehan, F. Claeyssens, S. Kelly, *Biomaterials* **2010**, *31*, 207.
[88] a) D. T. Simon, E. O. Gabrielsson, K. Tybrandt, M. Berggren, *Chem. Rev.* **2016**, *116*, 13009; b) B. D. Paulsen, K. Tybrandt, E. Stavrinidou, J. Rivnay, *Nat. Mater.* **2020**, *19*, 13.
[89] C. M. Proctor, J. Rivnay, G. G. Malliaras, *J. Polym. Sci., Part B: Polym. Phys.* **2016**, *54*, 1433.
[90] C. Kleber, K. Lienkamp, J. Rühe, M. Asplund, *Adv. Biosyst.* **2019**, *3*, 1900072.
[91] T. Niederhoffer, A. Vanhoestenberghe, H. T. Lancashire, *J. Neural Eng.* **2023**, *20*, 011002.
[92] S. Venkatraman, J. Hendricks, Z. A. King, A. J. Sereno, S. Richardson-Burns, D. Martin, J. M. Carmena, *IEEE Trans. Neural Syst. Rehabil. Eng.* **2011**, *19*, 307.
[93] J. Leal Ordonez, S. Shaner, L. Matter, C. Boehler, M. Asplund, *Adv. Mater. Interfaces* **2023**, *10*, 2202041.
[94] R. Valiollahi, M. Vagin, V. Gueskine, A. Singh, S. A. Grigoriev, A. S. Pushkarev, I. V. Pushkareva, M. Fahlman, X. Liu, Z. Khan, M. Berggren, I. Zozoulenko, X. Crispin, *Sustainable Energy Fuels* **2019**, *3*, 3387.
[95] K. Tybrandt, K. C. Larsson, S. Kurup, D. T. Simon, P. Kjäll, J. Isaksson, M. Sandberg, E. W. H. Jager, A. Richter-Dahlfors, M. Berggren, *Adv. Mater.* **2009**, *21*, 4442.
[96] K. Rohtlaid, G. Nguyen, C. Soyer, C. Eric, F. Vidal, C. Plesse, *Adv. Electron. Mater.* **2019**, *5*, 1800948.
[97] G. Dijk, H. J. Ruigrok, R. P. O'Connor, *Adv. Mater. Interfaces* **2020**, *7*, 2000675.
[98] J. Stejskal, I. Sapurina, *Pure Appl. Chem.* **2005**, *77*, 815.
[99] G. Cirić-Marjanović, E. Tomsik, M. Trchová, J. Stejskal, *Synth. Met.* **2008**, *158*, 200.
[100] P. Humpolíček, V. Kašpárková, J. Pacherník, J. Stejskal, P. Bober, Z. Capáková, K. A. Radaszkiewicz, I. Junkar, M. Lehocký, *Mater. Sci. Eng., C* **2018**, *91*, 303.
[101] J. Liu, Y. S. Kim, C. E. Richardson, A. Tom, C. Ramakrishnan, F. Birey, T. Katsumata, S. Chen, C. Wang, X. Wang, L. M. Joubert, Y. Jiang, H. Wang, L. E. Fenno, J. B. Tok, S. P. Paşca, K. Shen, Z. Bao, K. Deisseroth, *Science* **2020**, *367*, 1372.
[102] X. Strakosas, H. Biesmans, T. Abrahamsson, K. Hellman, M. S. Ejneby, M. J. Donahue, P. Ekström, F. Ek, M. Savvakis, M. Hjort, D. Bliman, M. Linares, C. Lindholm, E. Stavrinidou, J. Y. Gerasimov, D. T. Simon, R. Olsson, M. Berggren, *Science* **2023**, *379*, 795.
[103] X. Cui, V. A. Lee, Y. Raphael, J. A. Wiler, J. F. Hetke, D. J. Anderson, D. C. Martin, *J. Biomed. Mater. Res.* **2001**, *56*, 261.
[104] C. E. Schmidt, V. R. Shastri, J. P. Vacanti, R. Langer, *Proc. Natl. Acad. Sci. USA* **1997**, *94*, 8948.
[105] R. Green, M. R. Abidian, *Adv. Mater.* **2015**, *27*, 7620.
[106] X. B. Chen, J. P. Issi, J. Devaux, D. Billaud, *J. Mater. Sci.* **1997**, *32*, 1515.
[107] C. Boehler, S. Carli, L. Fadiga, T. Stieglitz, M. Asplund, *Nat. Protoc.* **2020**, *15*, 3557.
[108] a) J. Jang, J. Lee, S. Woo, D. J. Sly, L. J. Campbell, J.-H. Cho, S. J. O'Leary, M.-H. Park, S. Han, J.-W. Choi, J. Hun Jang, H. Choi, *Sci. Rep.* **2015**, *5*, 12447; b) I. Gablech, J. Klempa, J. Pekárek, P. Vyroubal, J. Hrabina, M. Holá, J. Kunz, J. Brodský, P. Neužil, *Micromachines* **2020**, *11*, 143; c) J. Segovia-Fernandez, S. Sonmezoglu, S. T. Block, Y. Kusano, J. M. Tsai, R. Amirtharajah, D. A. Horsley, presented at *2017 19th Int. Conf. Solid-State Sensors, Actuators and Microsystems (TRANSDUCERS)*, June **2017**.
[109] a) N. Aggarwal, S. Krishna, L. Goswami, S. K. Jain, A. Pandey, A. Gundimeda, P. Vashishtha, J. Singh, S. Singh, G. Gupta, *SN Appl. Sci.* **2021**, *3*, 291; b) X. Wang, T. Nguyen, Y. Cao, J. Jian, O. Malis, H. Wang, *Appl. Phys. Lett.* **2019**, *114*, 023103.
[110] a) C. Besleaga, V. Dumitru, L. M. Trinca, A. C. Popa, C. C. Negrila, Ł. Kołodziejczyk, C. R. Luculescu, G. C. Ionescu, R. G. Ripeanu, A. Vladescu, G. E. Stan, *Nanomaterials* **2017**, *7*, 394; b) N. Jackson, L. Keeney, A. Mathewson, *Smart Mater. Struct.* **2013**, *22*, 115033.
[111] I. Gablech, V. Svatoš, O. Caha, A. Dubroka, J. Pekárek, J. Klempa, P. Neužil, M. Schneider, T. Šikola, *Thin Solid Films* **2019**, *670*, 105.
[112] M. Pons, R. Boichot, N. Coudurier, A. Claudel, E. Blanquet, S. Lay, F. Mercier, D. Pique, *Surf. Coat. Technol.* **2013**, *230*, 111.
[113] a) K. Jagannadham, A. K. Sharma, Q. Wei, R. Kalyanraman, J. Narayan, *J. Vac. Sci. Technol., A* **1998**, *16*, 2804; b) K. A. Aissa, A. Achour, O. Elmazria, Q. Simon, M. Elhosni, P. Boulet, S. Robert, M. A. Djouadi, *J. Phys. D: Appl. Phys.* **2015**, *48*, 145307.
[114] a) M. Shakir, S. Hou, R. Hedayati, B. G. Malm, M. Östling, C.-M. Zetterling, *Electronics* **2019**, *8*, 496; b) A. Yi, C. Wang, L. Zhou, Y. Zhu, S. Zhang, T. You, J. Zhang, X. Ou, *Appl. Phys. Rev.* **2022**, *9*, 031302.
[115] A. Kashyap, C.-P. Chen, R. Ghandi, A. Patil, E. Andarawis, L. Yin, D. Shaddock, P. Sandvik, K. Fang, Z. Shen, R. Johnson, *Silicon Carbide Integrated Circuits for Extreme Environments*, IEEE, Columbus, OH, USA **2013**, pp. 60–63.
[116] a) M. Fraga, R. Pessoa, *Micromachines* **2020**, *11*, 799; b) O. Knotek, F. Löffler, L. Wolkers, *Diamond Relat. Mater.* **1993**, *2*, 528; c) V. Tiron, E.-L. Ursu, D. Cristea, G. Bulai, G. Stoian, T. Matei, I.-L. Velicu, *Nanomaterials* **2022**, *12*, 512. d) M. Skowronski, T. Kimoto, in *Handbook of Crystal Growth*, 2nd ed. (Ed: T. F. Kuech), North-Holland, Boston, MA **2015**.
[117] C. K. Nguyen, J. R. Abbott, S. Negi, S. F. Cogan, in *Annual Int. Conf. IEEE Engineering in Medicine and Biology Society*, Vol. *2021*, IEEE **2021**, p. 6623.
[118] F. Deku, Y. Cohen, A. Joshi-Imre, A. Kanneganti, T. J. Gardner, S. F. Cogan, *J. Neural Eng.* **2018**, *15*, 016007.
[119] S. F. Cogan, D. J. Edell, A. A. Guzelian, Y. Ping Liu, R. Edell, *J. Biomed. Mater. Res., Part A* **2003**, *67A*, 856.
[120] C. K. Nguyen, J. R. Abbott, S. Negi, S. F. Cogan, *43rd Annual International Conf. of the IEEE Engineering in Medicine & Biology Society (EMBC)*, IEEE, Mexico **2021**, pp. 6623–6626.
[121] H.-P. Phan, Y. Zhong, T.-K. Nguyen, Y. Park, T. Dinh, E. Song, R. K. Vadivelu, M. K. Masud, J. Li, M. J. A. Shiddiky, D. Dao, Y. Yamauchi, J. A. Rogers, N.-T. Nguyen, *ACS Nano* **2019**, *13*, 11572.
[122] C.-H. Lin, K. Komeya, T. Meguro, J. Tatami, Y. Abe, M. Komatsu, *J. Ceram. Soc. Jpn.* **2003**, *111*, 452.
[123] S. v. d. Driesche, C. Habben, A. Bödecker, W. Lang, M. J. Vellekoop, *Proceedings* **2017**, *1*, 299.
[124] a) S. Genter, O. Paul, Iop, presented at *14th Int. Conf. Micro- and Nano-Technology for Power Generation and Energy Conversion Applications (PowerMEMS)*, Hyogo, Japan, November **2014**; b) R. Caldwell, H. Mandal, R. Sharma, F. Solzbacher, P. Tathireddy, L. Rieth, *J. Neural Eng.* **2017**, *14*, 046011.
[125] J. Ortigoza-Diaz, K. Scholten, C. Larson, A. Cobo, T. Hudson, J. Yoo, A. Baldwin, A. W. Hirschberg, E. Meng, *Micromachines* **2018**, *9*, 422.
[126] T. Kremers, M. Tintelott, V. Pachauri, X. T. Vu, S. Ingebrandt, U. Schnakenberg, *Electroanalysis* **2021**, *33*, 197.
[127] T. Trantidou, M. Tariq, C. M. Terracciano, C. Toumazou, T. Prodromakis, *Sensors* **2014**, *14*, 11629.
[128] W. Shen, S. Das, F. Vitale, A. Richardson, A. Ananthakrishnan, L. A. Struzyna, D. P. Brown, N. Song, M. Ramkumar, T. Lucas, D. K. Cullen, B. Litt, M. G. Allen, *Microsyst. Nanoeng.* **2018**, *4*, 30.
[129] E. Berthier, E. W. K. Young, D. Beebe, *Lab Chip* **2012**, *12*, 1224.
[130] J.-M. Kim, C. Im, W. R. Lee, *Polymers* **2017**, *9*, 690.
[131] M. Wang, Y. Zhang, J. Bin, L. Niu, J. Zhang, L. Liu, A. Wang, J. Tao, J. Liang, L. Zhang, X. Kang, *Micromachines* **2022**, *13*, 1484.

[132] D. Koh, A. Wang, P. Schneider, B. Bosinski, K. W. Oh, *Micromachines* **2017**, *8*, 280.
[133] B. Osmani, H. Schift, K. Vogelsang, R. Guzman, P. M. Kristiansen, R. Crockett, A. Chacko, S. Bucher, T. Töpper, B. Müller, *Micro Nano Eng.* **2020**, *7*, 100051.
[134] G. Camino, S. M. Lomakin, M. Lazzari, *Polymer* **2001**, *42*, 2395.
[135] F. Decataldo, T. Cramer, D. Martelli, I. Gualandi, W. S. Korim, S. T. Yao, M. Tessarolo, M. Murgia, E. Scavetta, R. Amici, B. Fraboni, *Sci. Rep.* **2019**, *9*, 10598.
[136] K. M. Musick, D. J. Chew, J. W. Fawcett, S. P. Lacour, presented at *2013 6th Int. IEEE/EMBS Conf. Neural Engineering (NER)*, November **2013**.
[137] a) D. Güven, J. D. Weiland, M. Maghribi, J. C. Davidson, M. Mahadevappa, R. Roizenblatt, G. Qiu, P. Krulevitz, X. Wang, L. LaBree, M. S. Humayun, *Exp. Eye Res.* **2006**, *82*, 81; b) Q. A. Vu, H. W. Seo, K. E. Choi, N. Kim, Y. N. Kang, J. Lee, S. H. Park, J. T. Kim, S. Kim, S. W. Kim, *Front. Neurosci.* **2022**, *16*, 1010445; c) L. Ferlauto, M. J. I. A. Leccardi, N. A. L. Chenais, S. C. A. Gilliéron, P. Vagni, M. Bevilacqua, T. J. Wolfensberger, K. Sivula, D. Ghezzi, *Nat. Commun.* **2018**, *9*, 992.
[138] T. Liang, Y. Makita, S. Kimura, *Polymer* **2001**, *42*, 4867.
[139] M. Vomero, F. Ciarpella, E. Zucchini, M. Kirsch, L. Fadiga, T. Stieglitz, M. Asplund, *Biomaterials* **2022**, *281*, 121372.
[140] X. Jiang, X. Sui, Y. Lu, Y. Yan, C. Zhou, L. Li, Q. Ren, X. Chai, *J. NeuroEng. Rehabil.* **2013**, *10*, 48.
[141] D. A. Soscia, D. Lam, A. C. Tooker, H. A. Enright, M. Triplett, P. Karande, S. K. G. Peters, A. P. Sales, E. K. Wheeler, N. O. Fischer, *Lab Chip* **2020**, *20*, 901.
[142] D. Kuzum, H. Takano, E. Shim, J. C. Reed, H. Juul, A. G. Richardson, J. de Vries, H. Bink, M. A. Dichter, T. H. Lucas, D. A. Coulter, E. Cubukcu, B. Litt, *Nat. Commun.* **2014**, *5*, 5259.
[143] J. Badia, T. Boretius, D. Andreu, C. Azevedo-Coste, T. Stieglitz, X. Navarro, *J. Neural Eng.* **2011**, *8*, 036023.
[144] J. Gao, L. Guan, J. Chu, *Proc. SPIE* **2010**, *7544*, 754464.
[145] Z. Chen, J.-B. Lee, *Micromachines* **2021**, *12*, 794.
[146] H. Shin, Y. Son, U. Chae, J. Kim, N. Choi, H. J. Lee, J. Woo, Y. Cho, S. H. Yang, C. J. Lee, I.-J. Cho, *Nat. Commun.* **2019**, *10*, 3777.
[147] L. Luan, X. Wei, Z. Zhao, J. J. Siegel, O. Potnis, C. A. Tuppen, S. Lin, S. Kazmi, R. A. Fowler, S. Holloway, A. K. Dunn, R. A. Chitwood, C. Xie, *Sci. Adv.* **2017**, *3*, e1601966.
[148] M. Marelli, G. Divitini, C. Collini, L. Ravagnan, G. Corbelli, C. Ghisleri, A. Gianfelice, C. Lenardi, P. Milani, L. Lorenzelli, *J. Micromech. Microeng.* **2011**, *21*, 045013.
[149] A. Altuna, J. Berganzo, L. J. Fernández, *Front. Mater.* **2015**, *2*, 47.

Imrich Gablech studied Faculty of Electrical Engineering and Communication at the Brno University of Technology (BUT), Czech Republic (B.Sc. 2012, M.Sc. 2014) and defended his Ph.D. at Central European Institute of Technology (CEITEC) at BUT in study program Advanced Materials and Nanosciences (2018). He continued as a postdoc at CEITEC and was focused on thin film technologies, fabrication and characterization of MEMS devices and sensors. He works as a senior researcher in E. D. Glowacki group since 2021 and works on neural interfaces for which he benefits from previously gained skills in the field of microfabrication and MEMS.

Eric Glowacki studied chemistry at the University of Rochester, USA (B.Sc., M.Sc. 2009); and defended Ph.D. at the Johannes Kepler University, Linz, Austria, in physical chemistry (2013). He continued as a postdoc in Linz (2013–2016), with research interest moving into the field of electrophysiology. Between 2016 and 2020, he led a research group at Linköping University, Sweden, working on microfabricated neurostimulation devices. In 2020, he was awarded the ERC Starting Grant, with which he moved to CEITEC, Brno University of Technology, Czech Republic. His research is dedicated to neural interface technologies and bioelectronic medicine, and reactive oxygen species in physiology.